

THE LOCAL DYNAMICS OF BASEMENT MEMBRANE BREACHING DURING  
CANCER CELL INVASION

by

Shayan S. Nazari

A dissertation submitted to the faculty of  
The University of North Carolina at Charlotte  
in partial fulfillment of the requirements  
for the degree of Doctor of Philosophy in  
Biology

Charlotte

2022

Approved by:

---

Dr. Kenneth M. Yamada

---

Dr. Pinku Mukherjee

---

Dr. Didier Dreau

---

Dr. Julie Goodliffe

---

Dr. Gloria Elliott

©2022  
Shayan S. Nazari  
ALL RIGHTS RESERVED

## ABSTRACT

SHAYAN S. NAZARI. The local dynamics of basement membrane breaching during cancer cell invasion

(Under the direction of Dr. Kenneth M. Yamada)

Solid tumor metastasis is the leading cause of cancer-related mortality. Cancer invasion through the confining basement membrane (BM) is the initial step in tumor dissemination and metastasis, and it represents a key diagnostic feature of cancer. Thus, identifying the mechanisms involved in the breaching of cancer cells through the BM is potentially important for developing novel therapeutic approaches. BM is a dense sheet of specialized extracellular matrix proteins that separates tissue compartments. It is also a nanoporous structure, and since the average width of a cell is  $\sim 10 \mu\text{m}$ , invasion requires extensive widening of the BM nanopores. Previous research provided evidence that this expansion of BM nanopores involves protease degradation. However, protease inhibitors have failed to prevent cell invasion and metastasis in clinical trials, suggesting that cells may also breach the BM barrier using physical and mechanical mechanisms. Currently, it is unknown what mechanical mechanisms human tumor cells use to breach the BM. This is in part due to the difficulty of visualizing interactions at the cell-BM interface during cell invasion. Here, we designed and published a 3-dimensional *in vitro* organoid model of cancer spheroids encapsulated by a basement membrane and embedded in 3D collagen gels to visualize the early events of cancer invasion by confocal microscopy and live-cell imaging.

We first found that human breast cancer cells generated large numbers of basement membrane perforations, or holes, of varying sizes that expanded over time

during cell invasion. We used a wide variety of small molecule inhibitors to probe the mechanisms of basement membrane perforation and hole expansion. Protease inhibitor treatment (BB94), led to a 63% decrease in perforation size. After myosin II inhibition (blebbistatin), the basement membrane perforation area decreased by only 15%. These treatments produced correspondingly decreased cellular breaching events.

Interestingly, inhibition of actin polymerization dramatically decreased basement membrane perforation by 80% and blocked invasion. Our findings suggest that human cancer cells can primarily use proteolysis and actin polymerization to perforate the BM and to expand perforations for basement membrane breaching with a relatively small contribution from myosin II contractility.

We also found by using live timelapse imaging that cancer cells can send out long, actin-based prehensile protrusions (~30-100 microns in length) through the BM that subsequently grip and pull on the surrounding collagenous matrix to help cells pull themselves through the BM for invasion. These long protrusions are supported by microtubules and pull on the surrounding collagen using actomyosin contractility. We quantified this pulling exerted on collagen by generating kymographs for control and treatment groups and measuring collagen displacement over time. We found that by specifically inhibiting actin polymerization, microtubule formation, or actomyosin contractility, tumor organoids are unable to form these protrusions and fail to pull on the surrounding collagen matrix to enable invasion. Furthermore, by inhibiting the cell surface receptor for collagen, integrin  $\alpha 2\beta 1$ , organoids could not form protrusions nor pull on the surrounding matrix, indicating that protrusions use integrin  $\alpha 2\beta 1$  to attach to and pull on the collagen matrix during the initial stages of invasion through the BM. In

conclusion, some cancer cells extend long actin-based protrusions to bind to collagen via integrin  $\alpha 2\beta 1$  and use pulling forces driven by actomyosin contractility exerted on the surrounding extracellular matrix to squeeze through perforations in the basement membrane for translocating their cell body across this major tissue barrier to cancer invasion.

## **DEDICATION**

I would like to dedicate my dissertation to my family for their unconditional love and support. I would like to especially dedicate this dissertation to my mom, who against all odds left our home country and everyone we knew and loved, to bring me and my sisters here, so that we could have a better chance at becoming who we wanted to be. I hope I made you proud and that all the sacrifices you made over the years, was worth it.

## **ACKNOWLEDGEMENTS**

I would like to thank my family for their continuous and unconditional love and support throughout my entire life. My world is so much better with you in it. To my PhD adviser, Dr. Kenneth M. Yamada, thank you for allowing me to be a graduate student in your laboratory and shaping me as a scientist and hopefully a future mentor. I will never have another mentor like you again and the past three years have changed my life for the better. Thank you to all my PhD committee members for supporting me throughout my PhD journey at UNCC. To Dr. Mukherjee, your mentorship helped me get to where I am and your excitement for breast cancer research somehow took me from being very unsure of the direction of my career to having an actual path to follow through. I don't think I could have done it without you and I really thank you for that. Thank you to all the members of the Yamada laboratory. I am so grateful for every one of you, for the mentorship, the laughs and the many talks about science or life. Thank you to the Intramural Training and Education (OITE) program at NIH, the Graduate School and the Department of biological Sciences at UNC-Charlotte for providing me with funding and resources to complete my PhD.

## Table of Contents

LIST OF FIGURES.....	XII
LIST OF ABBREVIATIONS.....	XV
CHAPTER 1:.....	1
PREFACE.....	1
CELL-MATRIX INTERACTIONS IN CANCER.....	1
BASEMENT MEMBRANE .....	6
CELL MIGRATION .....	8
CELL PROTRUSIONS IN CANCER.....	9
INVASION BY CHEMICAL DEGRADATION (BASEMENT MEMBRANE BREACHING) .....	12
INVASION BY PUSHING FORCES AND CONTRACTILITY.....	13
CHAPTER 2:.....	17
GENERATION OF 3D TUMOR SPHEROIDS WITH ENCAPSULATING BASEMENT MEMBRANES FOR INVASION STUDIES.....	17
PREFACE.....	17
INTRODUCTION.....	18
BASIC PROTOCOL 1: GROWTH OF UNIFORMLY SIZED TUMOR SPHEROIDS WITH AN ENCAPSULATING BASEMENT MEMBRANE .....	23
BASIC PROTOCOL 2: POLYMERIZATION AND EMBEDDING OF TUMOR SPHEROIDS IN A 3D TYPE I COLLAGEN GEL .....	26
ALTERNATIVE PROTOCOL: EMBEDDING OF TUMOR SPHEROIDS IN COLLAGEN GELS USING A SANDWICH METHOD .....	31

BASIC PROTOCOL 3: FIXING AND IMMUNOSTAINING TUMOR SPHEROIDS	
EMBEDDED IN 3D COLLAGEN GELS .....	33
BACKGROUND INFORMATION .....	37
CRITICAL PARAMETERS .....	38
TIME CONSIDERATIONS .....	45
CHAPTER 3: .....	46
MECHANISMS OF BASEMENT MEMBRANE MICRO-PERFORATION DURING	
CANCER CELL INVASION INTO A 3D COLLAGEN GEL .....	
	46
PREFACE .....	46
INTRODUCTION .....	47
RESULTS AND DISCUSSION .....	51
Overview of the 3D-Spheroid Model .....	51
BM Encapsulated Spheroids before Invasion and Became Extensively Perforated in	
Our Three-Dimensional In Vitro Invasion Assay .....	55
BM Perforations Expanded over Time as Cancer Cells Initiated Invasion through	
the BM .....	59
Protease Activity Played a More Important Role than Actomyosin Contractility in	
Perforating the BM during Cancer Cell Invasion .....	62
Actin Polymerization Dramatically Affected Hole Formation and Acted as a Third	
Mechanism Contributing to Perforation of the BM .....	67
Comparisons with Other Cell Types Confirmed Findings for Another Metastatic Cell	
but Not for a Non-Metastatic Cell Line .....	70
CONCLUSIONS .....	74

CHAPTER 4: .....	75
LONG PREHENSILE PROTRUSIONS DISPLACE COLLAGEN AND PULL CELLS THROUGH THE BASEMENT MEMBRANE DURING CANCER INVASION.....	75
PREFACE.....	75
INTRODUCTION.....	76
RESULTS .....	78
Long cellular protrusions traverse the basement membrane before and during invasion and may apply traction to the surrounding matrix during BM breaching...	78
Cells pull on the surrounding collagen matrix through the basement membrane using myosin II .....	81
Actin polymerization and tubulin are necessary for long protrusion formation and stabilization of the protrusions for collagen displacement and ultimately cell invasion .....	87
Long protrusions attach to collagen via integrin $\alpha 2\beta 1$ to translocate the matrix during spheroid invasion .....	90
The role of proteases in protrusion formation, collagen displacement, and cell invasion .....	92
Characterizations of the long, prehensile-like, contractile protrusions .....	95
DISCUSSION .....	100
CHAPTER 5: .....	102
CONCLUSION AND PERSPECTIVE .....	102
MATERIALS AND METHODS .....	108

CELL CULTURE AND MEDIA .....	108
3-DIMENSIONAL SPHEROID CELL CULTURE .....	108
INHIBITORS .....	109
IMMUNOSTAINING .....	109
CONFOCAL IMAGING .....	109
LIVE CELL IMAGING .....	110
PERFORATION AREA ANALYSIS .....	110
COLLAGEN DISPLACEMENT ANALYSIS .....	111
STATISTICS.....	111
TWO-PHOTON CELL SEVERING.....	112
REFERENCES.....	113

## LIST OF FIGURES

### CHAPTER 1:

Figure 1.1. Matrix remodeling during tumor progression and mechanisms of cancer cell invasion.....	4
--	---

### CHAPTER 2:

Figure 2.1. Schematic representation of procedures for generating uniform spheroids with intact basement membranes and embedding them in 3D collagen gels for invasion studies.....	21
---	----

Figure 2.2. Spheroids with encapsulating basement membrane in 3D collagen gels.....	43
---	----

Table 2.1. Troubleshooting Guide.....	41
---------------------------------------	----

### CHAPTER 3:

Scheme 3.1. Schematic illustration of the protocol for generating cancer cell spheroids encapsulated in a basement membrane and embedded in a 3D collagen gel for invasion assays.....	52
--	----

Figure 3.1. Spheroid invasion through the basement membrane and into a collagen gel.....	54
--	----

Figure 3.2. Large perforations in the basement membrane appeared as cancer cells invaded.....	57
---	----

Figure 3.3. Basement membrane perforation over time.....	60
--	----

Figure 3.4. Contributions of proteolysis and myosin II contractility to basement membrane perforation.....	65
Figure 3.5. Contribution of actin polymerization to basement membrane perforation during collective cancer cell invasion.....	68
Figure 3.6. 4T1 spheroids show perforations in the basement membrane after 24 hours.....	72
Figure 3.7. A non-metastatic cell line does not generate large holes or invade into collagen gels.....	73

#### CHAPTER 4:

Figure 4.1. Timelapse live imaging of the spheroid invasion assay with confocal Imaging of long protrusions breaching the basement membrane.....	79
Figure 4.2. Collagen displacement requires myosin II contractility as does subsequent cell invasion.....	83
Figure 4.3. Extending long protrusions generate tension within the collagen microenvironment.....	85
Figure 4.4. Quantitative comparison of effects of actin polymerization inhibitors on rates of collagen displacement.....	88
Figure 4.5. Quantitative demonstration that the protrusions attach to collagen matrix via $\alpha 2\beta 1$ integrin.....	91

Figure 4.6. The role of proteases in spheroid protrusion formation, collagen displacement, and invasion.....93

Figure 4.7. Characterizations of the long protrusions.....97

Figure 4.8. Absence of myosin-X expression in the long thin protrusions.....99

CHAPTER 5:

Scheme 5.1. A model of basement membrane invasion.....107

## LIST OF ABBREVIATIONS

BB94	Batimastat
BM	Basement membrane
CAF	Carcinoma associated fibroblast
DMSO	Dimethyl Sulfoxide
ECM	Extracellular Matrix
EMT	Epithelial to mesenchymal transition
LOX	lysyl oxidase
MMP	Matrix metalloproteases
ROCK	Rho-associated protein kinase
TACS	termed tumor associated signature
Tg2	transglutaminase 2

## CHAPTER 1:

### Cell-matrix dynamics in cancer invasion

#### Preface

This chapter contains work from our recent publication in *Physical Biology* in 2022 in which I am a co-author, entitled “Cell-extracellular matrix dynamics” [1]. This article is published in an Open Access journal which allows for the use of its material with proper citation. This work is also a US Government work, therefore it is in the public domain in the USA. Andrew D. Doyle co-authored the first three sections of this review paper, and I was the primary author of the fourth section entitled “Cancer” in this published manuscript. Dr. Kenneth M. Yamada also contributed to the writing, major edits, and figure generation for this review paper.

#### Cell-matrix interactions in cancer

Overwhelmingly, the majority of cancer-associated deaths (about 90% of the cases) are caused by metastatic disease rather than primary tumors [2]. Cell migration is a critical step in both early embryonic morphogenesis and cancer cell invasion, which occurs through the dynamic processes of coordinated cell adhesion and contractility accompanied by proteolytic degradation and remodeling of the extracellular matrix (ECM) [3]. Invasive cancer cells are able to migrate away from the original tumor mass, traversing the confining basement membrane and through the 3-dimensional ECM by

means of single-cell migration or collective cell migration [4, 5]. For cancer cells to migrate and eventually metastasize, they must break through two sets of matrices: the basement membrane (BM) and the stromal extracellular matrix (ECM). BM and ECM have pores which can be much smaller than the size through which cells can migrate. Thus, for cells to acquire the ability to transmigrate through the matrix to invade and colonize surrounding tissue, they must be able to break through both the basal and stromal matrices.

In a tumor microenvironment, in-situ cancer cells are encased in a sheet of basement membrane surrounded by stromal extracellular matrix, which includes matrix proteins and stromal cells such as cancer-associated fibroblasts and immune cells. While cancer cells are physically separated by a basement membrane from stromal cells that surround the tumor, they can still communicate with stromal cells by secreting chemokines, cytokines, growth factors or crosslinking matrix components and matrix proteins, to affect stromal cells and their behavior. This increase in matrix deposition and crosslinking results in an increase in matrix density and stiffness, which commonly surrounds tumor tissue[6]. Cells accomplish crosslinking by secreting lysyl oxidase (LOX) and transglutaminase 2 (Tg2). LOX is typically overexpressed in the tumor microenvironment of many cancers, and it is often correlated with poor prognoses. CAFs and carcinoma cells also deposit increasing amounts of matrix proteins such as collagen I, fibronectin, laminin, osteopontin, and tenascin C in the tumor microenvironment, which results in a dense ECM termed desmoplasia [6] (Figure 1.1A). This increase in stiffness and density of the ECM alters the way in which cancer and stromal cells interact with their surrounding microenvironment and interestingly, cells

prefer to migrate toward a stiffer matrix in a process termed durotaxis [6-8]. Moreover, durotaxis is dependent on the function of lamellipodia and filopodial structures in an Arp2/3-dependent manner and independent of contact stimulation [8]. Another major observation was that collagen density and reorganization occur in stages that correlate with the progression of mammary tumors in a mouse model [9]. Provenzano and Keely describe the presence of dense, wavy collagen with thin fiber bundles around a small tumor, which they termed tumor associated signature 1 (TACS-1). The normal architecture of collagen is a wavy structure which allows for tissue deformation, involution, expansion during ductal growth and resistance to tension that can damage the tissue [9] (Figure 1.1B). TACS-2 describes the tumor that has increased in size with collagen fibers elongated and stretched in parallel around the boundary of the tumor (Figure 1.1B). While the wavy fibers served the purpose of supporting the growth of the normal gland, straight collagen fibers could act as shuttles for transmitting mechano-signals across the basement membrane. TACS-3 describes the regions of the tumor in which local invasion has occurred; collagen fibers were shown to be perpendicular to the tumor boundary (Figure 1.1B). At this stage, collagen fibers are aligned and oriented 90 degrees to the tumor boundary where local invasion is present. This could suggest that CAFs are actively aligning the matrix to allow for cancer cells to use these fibers as tracks for cell invasion. In a 3-dimensional in vitro model of high collagen density, normal mammary MCF10A cells show a more invasive morphology and expression of known EMT (epithelial-mesenchymal transition) markers in higher density collagen gels, compared to lower concentration of collagen I gels [10]. This could suggest that tissue density and architecture is an important culprit in tumor progression.

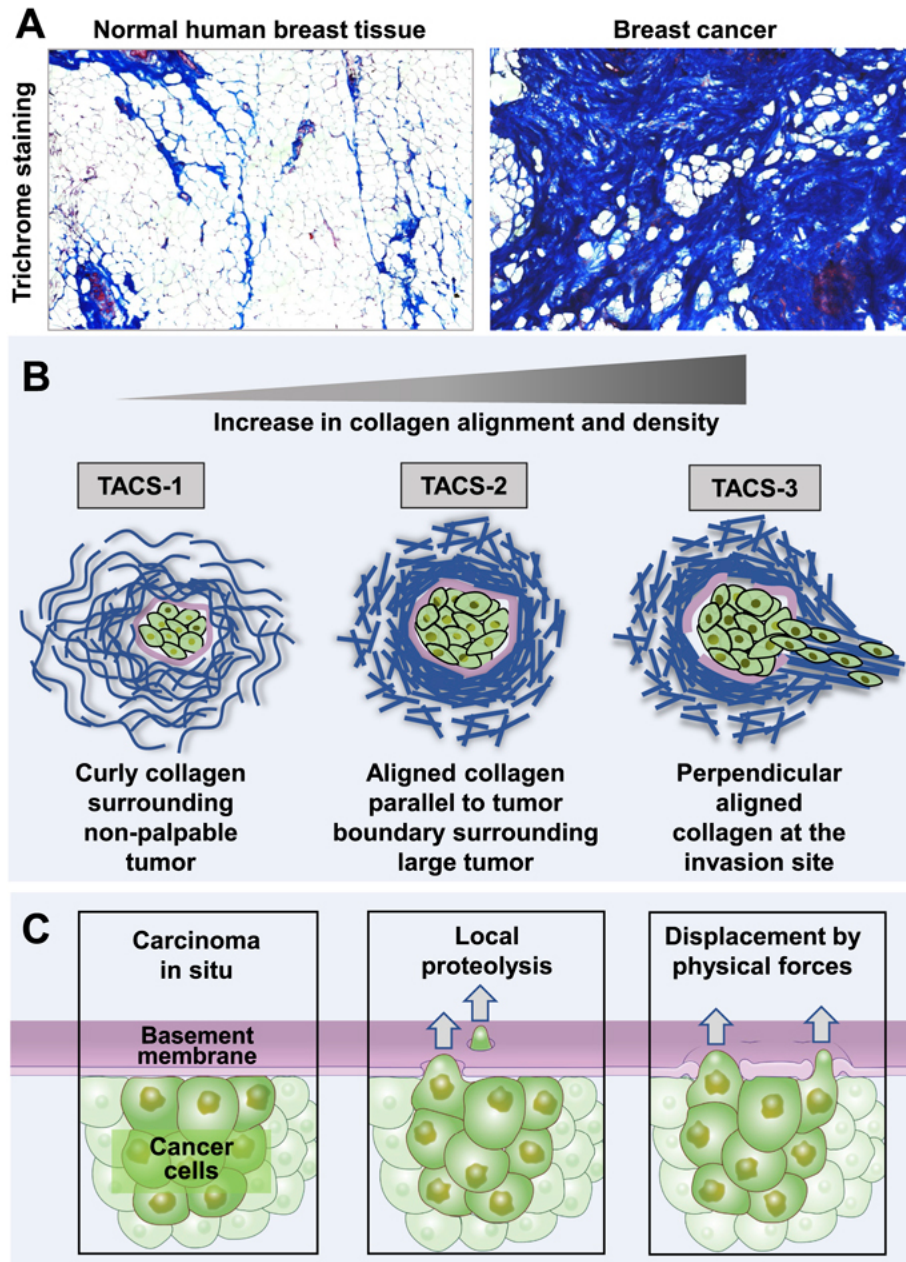


**Figure 1.3. Matrix remodeling during tumor progression and mechanisms of cancer cell invasion.**

(A) Breast cancer progression correlates with higher collagen density demonstrated by trichrome blue staining to measure collagen density in normal compared to tumor tissue from the same patient. (B) Matrix remodeling closely correlates with tumor progression.

Normal curly collagen fibrils surround a non-palpable tumor with localized collagen density around the periphery of the tumor mass (TACS-1). As the tumor enlarges, collagen is remodeled and appears more linear, dense, and aligned parallel to the tumor boundary (TACS-2). During cancer cell invasion, collagen becomes perpendicular to the tumor boundary at the invasion site (TACS-3). (C) During cancer invasion, cancer cells can breach the basement membrane barrier by chemically degrading the matrix using proteolysis or physically displacing the matrix by pushing through the basement membrane using invasive protrusions. (*This figure is taken directly from our publication in Physical Biology with permission from the authors [1]*).

## **Basement membrane**

Basement membrane penetration is an important initial step in invasion and hematogenous dissemination, leading to tumor metastasis and decreased patient survival. Since tumor metastasis is responsible for the high mortality rates in breast cancer and other malignancies, studying the initial steps of invasion through the basement membrane is important for therapeutic discoveries and metastasis prevention measures.

Basement membrane is a thin, sheet-like network of proteins, composed of laminin, collagen IV, perlecan, nidogen and proteoglycans. Laminin directly binds to cell surface receptors such as  $\beta$ 1 integrin and dystroglycan and self-assembles into a dense sheet. Collagen IV then polymerizes to form a second covalently crosslinked network [11]. Collagen IV polymers associate with laminin polymers via nidogen/entactin crosslinks. Basement membrane serves as a structural layer, encapsulating epithelial and endothelial cells [12-14]. Basement membrane is a nanoporous structure. These nanopores restrict movement and diffusion of large molecules through the BM, while allowing for permeability of small molecules. The sizes of the BM pores vary depending on the tissue type, with the average pore size (the distance between fibers in three dimensional space) of mammary epithelial BM measured to be ~10 nm [12, 15]. During local cell invasion, cancer cells infiltrate through basement membrane pores and migrate in the ECM toward the circulatory or the lymphatic system. Since cells are ~10 microns, with the nucleus being the largest portion of the cell, for invasion to occur, cells need to widen the nanometer-sized pores of the basement membrane to invade [12]. This expansion of pores requires protease degradation of the basement membrane and the

surrounding stroma ECM. Furthermore, basement membrane degradation also results in the release and activation of growth factors involved in angiogenesis, tumor invasion, and metastasis. Localized basement membrane degradation requires the secretion of matrix metalloproteases (MMPs) which also include the family of ADAMs (a disintegrin and metalloproteinase). MMPs are a family of zinc endopeptidases that cleave ECM molecules. ADAMs are enzymes that cleave growth factors, cytokine receptors, and adhesion molecules. MMPs, on the other hand, are important enzymes for ECM remodeling during wound healing, development, mammary gland involution, and angiogenesis. It is believed that cancer cells form mechanosensitive actin-based protrusions called invadopodia that deliver proteases for ECM protein degradation and thereby enable penetration through the basement membrane [16-19]. Invadopodia are 0.5 to 2 microns in width and protrude up to 2 microns in length from the surface of the cell and contain concentrations of the membrane-bound protease MT1-MMP [17].

## Cell migration

Cell migration is vital for normal tissue formation, maintenance, and regeneration. For the majority of cell types including epithelial, stromal and neuronal cells, cell migration generally occurs during tissue morphogenesis but can restart during wound healing [20]. Epithelial cells generally move along a basement membrane but are kept separated from the extracellular matrix, while other cells such as leukocytes can move through the stroma, blood vessels or other tissues in the body. Cell migration also plays a vital role in cancer cell invasion and dissemination and ultimately tumor metastasis [20].

Cells can migrate individually or collectively. The mode of migration that cells use can depend on a number of factors including, but not limited to, the extracellular environment, cell morphology and the presence of protrusions or cell-rounding, expression of integrins and proteases, and the ability to generate force to reorganize the matrix. Most different modes of cell migration *in vivo* occur in a three-dimensional setting, although cells can also migrate in a two-dimensional sheet such as during wound healing. On 2D surfaces, cell migration has been described as involving several steps, which involve establishing cell polarity by forming a lamellipodium at the front of the cell which is a branched network of actin filaments catalyzed by Arp2/3 complex [21, 22]. This extension of the front of the cell is followed by adhesion to the underlying substrate using integrins and a retrograde flow of actin to initiate forward movement and actomyosin-mediated retraction of the trailing edge of the cell. During cell migration on a 2D surface, cells can adhere to and apply forces upon a single, uniformly rigid surface. In contrast, in a 3D microenvironment, cell migration is vastly different due to the fact

that epithelial cells (among other cell types) are anchored to a basement membrane that separate tissues and organs from the underlying extracellular matrix, a complex three-dimensional network of fibrillar collagens with varying sizes of pores that allow for diffusion of molecules. Thus, it is not surprising that cells adopt a variety of migration patterns in 3D matrices and have different morphological appearances with varying protrusions and mechanisms. Cells in 3D are incredibly plastic and can change morphology and behavior depending on extrinsic and intrinsic factors [23].

### **Cell protrusions in cancer**

Cell protrusions can control the activity of the leading edge of the cell and the direction of its movement. The protrusions of lamellipodia, pseudopodia, and filopodia that attach the cell to underlying extracellular matrix are regulated by the small GTPases Cdc42 and Rac. The lamellipodium is an actin-based protrusion in 2D, and the mechanisms of its roles in 2D migration have been thought to also parallel mesenchymal cell migration, which occurs in cancer cells *in vivo* after epithelial-to-mesenchymal transition leading to basement membrane invasion. Lamellipodium extension in mesenchymal cell migration is controlled by high Rac activity. Arp2/3 activity and lamellipodia formation have been implicated in cancer metastasis in mouse models and human patients, by promoting actin polymerization through WAVE, cell protrusion formation and cancer dissemination. Similarly, overexpression of the downstream WASP family complex is associated with poor clinical outcomes, and a decrease in expression of a negative regulator of Arp2/3, Arpin, is also linked to poor breast cancer prognosis [21, 24].

In cancer cells, increased lamellipodial activity is positively correlated with 3D cell migration, invasion, and metastasis, but other studies have shown that additional F-actin-based protrusions can complement or compensate to promote 3D migration [21]. Filopodia are actin-based protrusions that are formed through Cdc42 activation and have been reported to play a role in cell migration, sensing the environment chemically or physically, and assisting cell-cell adhesion [21]. Myosin-X is expressed in filopodia, and it is induced by gain-of function mutant P53 and is shown to play a role in breast and pancreatic cancer metastasis leading to poor outcomes [25]. Filopodia have been implicated in cell migration and invasion in 3D during development and cancer. These protrusions are known to initiate contact with the ECM in metastatic breast cancer cell lines via Rho-GTPase-formin, to induce adhesion formation and proliferation via ERK and thus promoting tumorigenesis [21, 26].

Another protrusion that is important for cell invasion is the formation of actin-rich protrusions called podosomes or invadopodia. Podosomes are generally described in normal cells, and invadopodia have been shown in cancer cells. While these two structures are both actin-based processes with the ability to degrade the matrix, they differ in their size, location and duration [27]. Invadopodia are usually observed in cells that have been oncogenically transformed, and they tend to protrude further into the matrix during invasion compared to podosomes, which do not invade or cross a basement membrane. Cells use invadopodia to secrete matrix-degrading enzymes such as matrix metalloproteinases (MMPs) with the goal of locally degrading the matrix during invasion and migration by secreting or expressing matrix-degrading enzymes such as MMPs [27]. Invadopodia are typically marked by the expression of cortactin,

Tks4, and Tks5. The internal structure of invadopodia also includes the actin nucleating complex, ARP2/3-WASP (Wiskott-Aldrich syndrome protein) and interacting proteins such as cortactin, cofilin, fascin, and Rho-GTPases. The length and width of invadopodia are time dependent, and they can increase up to 2 microns in length and their width can also fluctuate between 0.5-2 microns. Moreover, the length of invadopodia has been shown to also increase to 20 microns in 3D cultures compared to traditional 2D cultures. Collagen density and concentration can also have an effect on the length of the invadopodia[12].

Formation of invadopodia can be described in three stages: initiation, assembly, and maturation, which is fully explained in detail in a comprehensive review by Jacob and Prekeris [27]. In brief, at the initiation phase, an actin-based “bud” is formed at cell’s edge protruding through the basement membrane and marking the initial breaching stage. This process can be initiated by chemical stimuli such as growth factors, as well as physical constraints such as high matrix density [28]. This initial signal leads to the activation, phosphorylation, and recruitment of many key proteins such as Src, Arg, cortactin, Nck1, and Neural Wiskott-Aldrich syndrome protein (N-Wasp). The activation of N-Wasp through Cdc-42 leads to actin polymerization through an N-Wasp/Arp 2/3 complex, resulting in “bud” formation, which marks the initial invadopodia initiation step [27]. What triggers and accelerates invadopodia activation and length is desmoplastic stroma, described as a collagen-rich environment that is usually observed in regions around solid tumors. These highly dense fibrillar collagen accumulations in the tumor microenvironment have been shown to induce invadopodial activation [28]. At the assembly stage, several proteins are recruited to the invadopodia “bud” to induce

nucleation of branched actin proteins and convert the “bud” to a mature invadopodium. At the maturation stage, actin polymerization forming branched and linear networks is still essential to invadopodia formation. Dia2, a formin, and fascin are important proteins that promote further invadopodia elongation during the maturation stage [27]. Moreover, beta 1 integrin is also present in invadopodia for collagen IV degradation[27]. At the final maturation stage, there is also a presence of microtubules in the invadopodia, which could act as a source of stability for the protrusion. There are also vesicles present which may contain proteases important for matrix degradation and invasion [27]. Three important matrix metalloproteinases (MMPs) that are found to be concentrated in invadopodia are MMP2, MMP9, and MMP14 (or Mt1-MMP).

### **Invasion by chemical degradation (basement membrane breaching)**

In general, there are 6 types of proteases, including matrix metalloproteases (MMPs), cysteine, serine, glutamic acid, threonine and aspartate proteases. All of them may be involved in cancer invasion and progression [12]. However, MMPs are thought to be especially important during BM breakdown and cancer migration and invasion [12]. MMPs are zinc-dependent endopeptidases categorized into groups according to their substrates. There are a number of MMPs, more than 20, some that are secreted and others are membrane-bound. A post-transcriptional regulations of MMP activity is that they must be activated from their precursor form of the MMP and can be inhibited while in their active form, by tissue inhibitors of metalloproteinases (TIMPs) [29]. MMPs are synthesized as an inactive pro-enzyme through the interaction of a cysteine-bound motif at the pro-peptide domain with the zinc-ion at the catalytic site. MMPs are

activated extracellularly by the removal of the pro-peptide domain [27, 29]. MMP expression is correlated with increased cancer invasion, advanced tumor stage, metastasis, and higher mortality. The expression of the three membrane-bound MMPs MT1-MMP (MMP-14), MMP15 and MMP16 was found to be especially important in tumor cell invasion of an ex vivo mouse model of BM and cell-derived BM matrix [30]. Another interesting recent finding was that MT1-MMP, which is known to be present in the invadopodium to chemically degrade the matrix, also can bind to collagen fibers and initiate a signaling cascade leading to Tks5 recruitment and actin polymerization at the protrusion, leading to pushing force-mediated invasion [17].

### **Invasion by pushing forces and contractility**

Traditionally, it was thought that cell relied on chemical degradation of the basement membrane, through MMPs, as the only mechanisms to breach through during invasion. However, emerging evidence has shown that there may be mechanical mechanisms that cells use to transmigrate through during cancer invasion. A number of clinical trials that used broad spectrum or more specific MMP inhibitors failed to diminish mortality [31-33], While there are a number of other explanations for the failure of the clinical trials such as dosing, side effects, advanced stage of cancer and inhibitor specificity, these findings suggests that while tumor cells can proteolytically remodel the matrix, they must also use force to mechanically organize the ECM as they move through the fibers, which thus plays a crucial role during cancer progression [12] (Figure 1.1C).

In general, there are two different force-generated movements that can lead to cell migration: pushing force of the cell body and the pulling force at the ECM [20]. Actin polymerization leading to the pushing force of the plasma membrane is observed in the protrusion of the leading edge. In collective cell migration, leader cells must generate force through actomyosin contractility by Rho GTPase signaling, and integrin-mediated traction on the ECM [22, 34]. Increased expression of Cdc42 and ROCK-induced actomyosin contractility is found at the edge of invading tumor cells [34, 35]. During collective cell migration, follower cells use actomyosin-dependent pulling force to maintain force between the matrix and the follower cell and to maintain the grouping between cells to retain forward movement [34].

Carcinoma associated fibroblasts (CAFs), a type of stromal cell present in the ECM, remodels the matrix independent of proteolysis [36]. CAFs were able to only widen pre-existing holes that were perforated via proteolysis or pre-existing breaks in the BM. Invasion of cancer cells was also not dependent on the softness of the matrix, but it instead depended on contractility [36]. Interestingly, CAFs are also shown to act as leader cells and leave “microtracks” behind them for cancer cells to follow during invasion [6]. During cancer cell invasion, stromal cells in the tumor microenvironment such as cancer associated fibroblasts (CAFs) and macrophages have been documented to exert force and remodel the basement membrane, open pre-existing pores in the BM, or leave micro-tracks for cells to follow and result cancer cell invasion [36, 37]. What is still under debate is whether force-driven breaching by invading cells themselves is equally important in cancer cell invasion and transmigration. In a *Caenorhabditis elegans* model of invasion, anchor cells use force generated by an actin network via the Arp2/3

complex to deform and displace the basement membrane, which was evident by the increase in signal around the BM perforation [14]. Interestingly, the MMP-devoid invadopodia increased in size by 5 times compared to normal invadopodia and were rich in ARP2/3, ATP, and mitochondria[14]. Similarly, a recent paper demonstrated MMP-induced perforations in the basement membrane of the embryo during early embryonic development [38]. Moreover, during salivary gland morphogenesis, epithelial cells use myosin II to perforate the basement membrane and as a result translocate the matrix around the perforated area [11]. Myosin II inhibition led to a local discontinuation of tugging at the tip of the bud, and it also globally inhibited the perforation of the BM surrounding the bud, highlighting the importance of epithelial cells' capability to interact with their basement membrane resulting in invasion [11].

Myosins are actin motor proteins that functionally depend on hydrolysis of ATP to generate force for cell contractility, cell signaling, and vesicle trafficking (among other roles). All myosins have a head domain that bind domain and is responsible for the ATPase activity of myosin. The neck domain which can bind light chains and a tail chain, which can vary in length depending on myosin's function [39]. Myosin II is a class of myosins that includes muscle myosins, responsible for contraction of sarcomeres, and non-muscle myosins, implicated in force-generation [39]. Non-muscle myosins are important for a variety of cellular structures, such as microvilli, filopodia, and adhesion belts. Ouderkirk and Krendel [39] have a very detailed review on myosins in cancer. The genes that encode non-muscle myosin II heavy chain in humans are MYH9 or myosin IIA, MYH10 or myosin IIB, and MYH14 or myosin IIC. Non-muscle

myosin IIA and IIB are both implicated in actin stress fibers and regulating cell contractility, cell migration both may contribute to tumor invasion[39].

Basement membrane perforation during cell invasion has been demonstrated in *C. elegans* mode[40], during mouse salivary gland morphogenesis[11], and in mouse embryogenesis [38], as an initial event in basement membrane breaching. Protease-independent cell invasion and migration via actomyosin contractility has also been studied using single cells or cells that have already invaded into the matrix. Collective cell invasion and migration is observed in epithelial solid tumors, utilizing the same mechanisms that are observed in morphogenesis and development; however, the exact mechanisms that cancer cells use to transmigrate through a basement membrane, during cancer invasion, is still unclear. In this dissertation, we aimed to understand how cancer cell spheroids, in a collective form, interact with their surrounding extracellular matrix and their immediate barrier, the basement membrane, as they are transmigrating through the basement membrane, in the early stages of cancer invasion. We hope that these studies will ultimately contribute to creating therapeutic targets for blocking tumor invasion and metastasis.

## CHAPTER 2:

### Generation of 3D Tumor Spheroids with Encapsulating Basement Membranes for Invasion Studies [41]

#### Preface

The work in this chapter is from the work that was published by Wiley publishing in *Current Protocols in Cell Biology* in 2020, entitled “Generation of 3D Tumor Spheroids with Encapsulating Basement Membrane for Invasion Studies” [41]. This article is the *in vitro* model and thus the bases in which the rest of my dissertation work builds upon. I am the first author and the corresponding author in this article. I designed the experiments and carried them out and conducted troubleshooting throughout. Major editing, oversight, and contribution to the idea of this *in vitro* model was provided by my PhD advisor, Dr. Kenneth M. Yamada.

Copyright permission has been granted by the Copyright holder to use this manuscript in my dissertation. This is an open access article under the terms of the <http://creativecommons.org/licenses/by-nc-nd/4.0/> License, which permits use and distribution in any medium, provided the original work is properly cited, the use is non-commercial and no modifications or adaptations are made. This chapter is also a US Government work, therefore it is in the public domain in the USA.

## Introduction

In the normal mammary gland, epithelial cells that line the lumen are adjacent to contractile myoepithelial cells that surround them peripherally. The epithelial and adjacent contractile cells are encased in a supportive basement membrane. At the initial stage of a mammary tumor, ductal carcinoma in situ (DCIS) premalignant epithelial cells proliferate into the ductal lumen but remain confined within the basement membrane [42, 43]. In contrast, during mammary tumor progression into invasive ductal carcinoma (IDC), there is a loss of the myoepithelial cell layer and a marked breaching of malignant cells through the basement membrane [42].

Cell migration is a critical step in early morphogenesis and in cancer cell invasion, which occurs through dynamic processes of synchronized cell adhesion and contractility, resulting in degradation and remodeling of the extracellular matrix (ECM) [3]. Invasive cancer cells are able to migrate away from the original tumor mass, traversing the confining basement membrane and moving through the three-dimensional (3D) ECM by means of single-cell migration or collective cell migration [4, 5]. Basement membrane penetration by cancer cells is an important initial step in invasion and hematogenous dissemination, leading to tumor metastasis and decreased patient survival. Since tumor metastasis is responsible for the high mortality rates in breast cancer and other malignancies, studying the initial steps of invasion through the basement membrane is important for therapeutic discoveries and prevention of metastasis.

To understand the initial stages of cancer cell invasion and migration, many researchers have started to use 3D hydrogels to mimic the ECM. For years, 2D cell cultures in monolayers were the standard for studying cancer cell biology and testing drug treatments and immunotherapies in vitro [44]. For decades, 2D cell cultures provided valuable insights for deciphering the mechanisms of cellular migration and identifying the key players involved in unicellular and multicellular cell adhesion and cell motility [45, 46]. However, 2D cultures fail to fully recapitulate the dimensionality of the breast cancer microenvironment and those of other malignancies. Moreover, studies have demonstrated differences in cellular morphologies and cellular signaling between 2D and 3D culture systems [23]. To overcome this obstacle, in vitro 3D tumor models have emerged in recent years as a superior method for studying the mechanisms of cancer initiation and progression. Many laboratories have used a mixture of Matrigel and collagen I gel to model basement membrane–ECM–cell interactions [10, 43]. Here we describe a protocol for generating uniform mammary tumor spheroids with an intact basement membrane embedded in a 3D collagen gel for invasion studies. Since DCIS is shown to form overwhelmingly in the areas of the breast that are more radiologically dense, with increased ECM stiffness and higher collagen I expression [47, 48], we use type I collagen gels, extracted from rat tail, to model the collagen-rich ECM.

In this article, we describe three main protocols for mammary tumor invasion studies (Fig. 1): (1) generation of uniform mammary tumor cell spheroids with an encapsulating basement membrane (see Basic Protocol 1), (2) polymerization of collagen type I from rat tail and embedding of the tumor spheroid in the 3D collagen gel (see Basic Protocol 2), and (3) fixing and immunostaining of the spheroid (Basic

Protocol 3). Although described for mammary cells, these protocols could be readily extended to other cancer cell types.

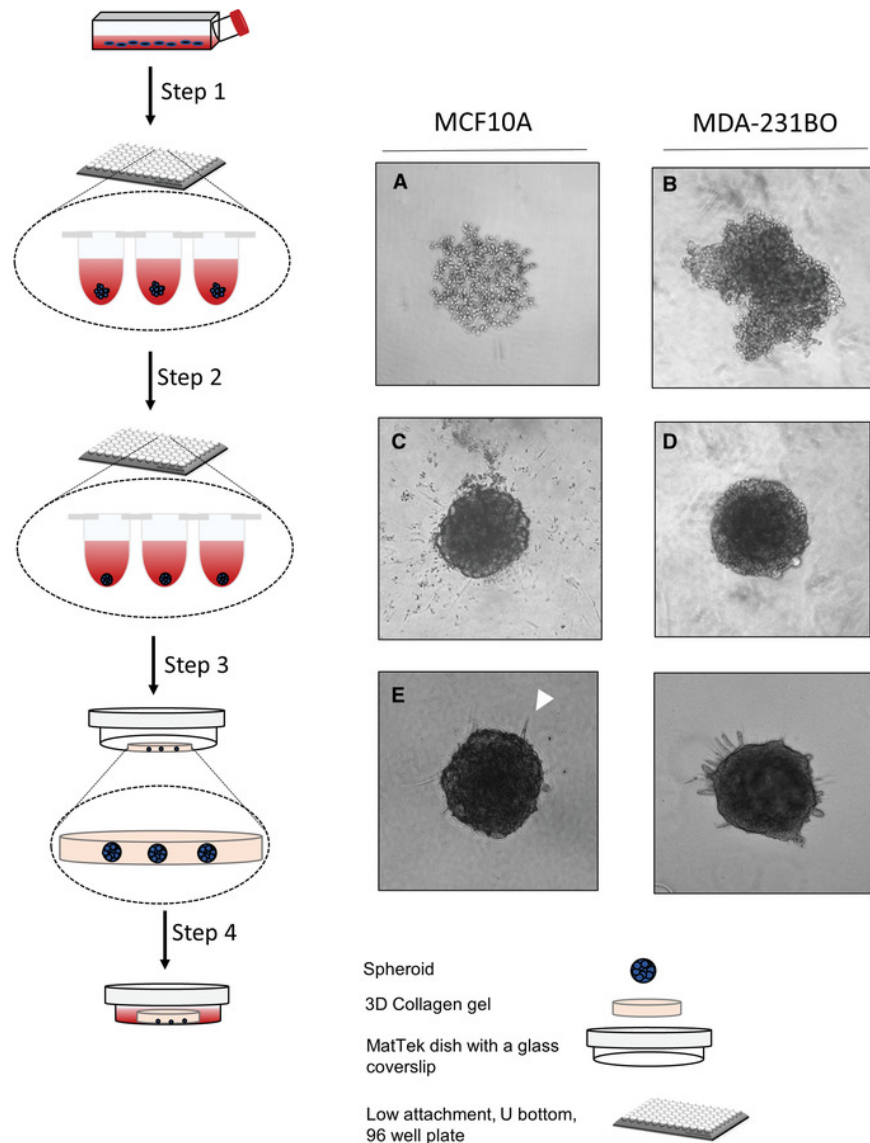


**Figure 4.1. Schematic representation of procedures for generating uniform spheroids with intact basement membranes and embedding them in 3D collagen gels for invasion studies.**

(1) Seed 2000 cells per well in a low-attachment 96 well U-bottom plate. After centrifugation, aggregates form in the wells (A and B). (2) Adding 5% Matrigel solution results in a conversion of the aggregates into well-formed spheroids in the wells

(C and D). (3) After neutralizing the collagen gel, embed the spheroids in the collagen gels in MatTek dishes. Allow the gel to polymerize at 37°C for 30 min. (4) Add fresh medium to the dishes and allow cells to invade into the collagen-rich ECM after 48 hr (E and F).

## ***Basic Protocol 1: GROWTH OF UNIFORMLY SIZED TUMOR SPHEROIDS WITH AN ENCAPSULATING BASEMENT MEMBRANE***

During DCIS, a premalignant stage in breast cancer, cells remain within the basement membrane and the myoepithelial cell layer, but invasive cells start to grow into the duct. This stage is also accompanied by deposition, linearization, and thickening of collagen I fibers, resulting in increased ECM stiffness [42]. Progression to IDC from DCIS involves the breach of tumor cells through the basement membrane and further stiffness of the surrounding ECM. To model DCIS and the first stage in mammary cancer progression, we demonstrate a method for growing uniform spheroids with an intact basement membrane surrounding the spheroid. For the purpose of this protocol, we use two cell lines (MCF10A and MDA-231BO) to show the method and the possible variability of the basement membrane surrounding the spheroids. MDA-231BO cells [49] were a gift from Dr. Kandice Tanner.

### **Materials**

Cell lines and culture media:

MCF10A cells (ATCC, cat. no. CRL-10317) with supplemented DMEM/F12 for MCF10A cells

MDA-231BO cells (kind gift from Dr. Kandice Tanner, National Cancer Institute, NIH) with supplemented DMEM for MDA-231BO cells

Matrigel, growth factor–reduced, phenol red–free (Corning, cat. no. 356231)

200- $\mu$ l multichannel pipettor (e.g., Gilson) with reservoirs

Costar ultra-low-attachment U-bottom 96-well plates (Sigma-Aldrich, cat. no. CLS7007)

Humidified incubator at 37°C with 10% CO<sub>2</sub>

Benchtop centrifuge for plates (e.g., Eppendorf 5810R) at room temperature

**Protocol steps — *Step annotations:***

**Day 1**

1. Using a multichannel pipettor, seed 2000 cells per well in sterile ultra-low-attachment U-bottom 96-well plates. Culture for 8-16 hr in a humidified 37°C, 10% CO<sub>2</sub> incubator. Calculate the number of cells needed based on a final volume of 200 µl per well. Include enough for at least ten extra wells when using a multichannel pipettor.

**Day 2**

2. Centrifuge plates for 5 min at 18 × g, 25°C to initiate aggregation of cells within each well.
3. Incubate at 37°C for 2 days to allow cells to grow and form more compact aggregates.

**Day 3**

4. Thaw Matrigel basement membrane matrix by leaving it overnight at 4°C in the back of a refrigerator or in a cold room. Matrigel can begin to polymerize and form small clumps if not thawed slowly overnight. The process described above ensures that

the Matrigel will thaw gradually and yield a homogeneous solution when added to the wells. Leaving pipette tips in the refrigerator overnight for handling the Matrigel also helps ensure that the Matrigel will not polymerize prematurely during pipetting.

#### **Day 4**

5. Remove 100  $\mu$ l medium from each well using a multichannel pipettor, being careful to touch the pipet tips to the inside wall of each well before slowly aspirating.
6. Prepare a 10% (v/v) Matrigel solution by diluting the stock in ice-cold supplemented DMEM/F12 medium (concentration 7.1 mg/ml).
7. Pipet 100  $\mu$ l of 10% Matrigel into each well, making the final Matrigel concentration 5% compared to the original stock.
8. Centrifuge plates for 5 min at  $18 \times g$   $25^{\circ}\text{C}$ . It is important to centrifuge plates at  $25^{\circ}\text{C}$ . Centrifuging at  $4^{\circ}\text{C}$  during this step will result in patchy assembly of basement membrane around the spheroids.
9. Return to incubator and allow spheroids to grow for 2 days after addition of Matrigel.

You should see formation of very round spheroids the next day, but 2 days are needed to ensure adequate assembly of basement membrane components around the spheroids. If you let spheroids grow for only 1 day, the basement membrane will look patchy when immunostained.

## ***Basic Protocol 2: POLYMERIZATION AND EMBEDDING OF TUMOR SPHEROIDS IN A 3D TYPE I COLLAGEN GEL***

During cancer progression, invasive cancer cells invade through the basement membrane and migrate through the ECM microenvironment, which generally consists primarily of collagen type I protein. DCIS has been shown to form in more mammographically dense tissue with increased collagen density [48]. Collagen I is known to be a cellular signaling and proliferative molecule, as shown by the Keely lab [50], but linear collagen type I in the ECM can also act as a highway on which invasive cancer cells can crawl and migrate [9, 51]. Here, we describe a method for embedding 3D tumor spheroids with an intact basement membrane in a collagen type I gel for invasion studies.

Before beginning, the detailed protocols of Dr. Andrew Doyle are used to isolate rat tail collagen I (see Current Protocols article:[52]), label collagen gels [53], and acid wash and activate MatTek dishes by salinization (see Current Protocols article:[54]) to ensure that the collagen gels remain adherent to the bottom of the dish and that cells do not preferentially adhere directly to the dish. It is critical that these protocols be followed exactly.

### ***Materials***

Dulbecco's PBS with calcium and magnesium (DPBS; HyClone, cat. no. SH30264.02)

6.0 mg/ml rat tail collagen stock solution in 20 mM acetic acid (see Current Protocols article: [52])

10× DMEM

10× reconstitution buffer

1 N NaOH

96-well U-bottom plate with spheroids (see Basic Protocol 1)

Hanks' balanced salt solution (HBSS; Current Protocols, 2001

Culture medium (see Basic Protocol 1)

1.5-ml microcentrifuge tube

Ceramic tile (large enough for a MatTek dish)

Positive-displacement pipettors and pipet tips

pH strips (e.g., MColorpHast, pH range 6.5-10, Millipore-Sigma, cat. no.

1.09543.0001) Inverted microscope

MatTek dishes (35 mm, no. 1.5 coverslip, 20-mm opening; cat. no. P35G-1.5-20-

C), acid-washed and silanized (see Current Protocols article: [54])

Humidified incubator at 37°C with 10% CO<sub>2</sub>

### **Prepare neutralized collagen**

1. Place a 1.5-ml microcentrifuge tube and a ceramic tile in a rectangular ice dish to chill. Also place DPBS, collagen stock solution, and aliquots of 10× DMEM, 10× RB, 1 N NaOH, and 1 N HCl on ice. The tile will provide a smooth surface on

which the MatTek dishes will be placed on ice and kept cold. The tube will be used for neutralizing the acidic collagen solution.

2. Calculate the volume of 6.0 mg/ml stock collagen ( $V$  collagen) needed to give 200  $\mu$ l per dish of 4 mg/ml neutralized collagen. For two dishes:

$$V \text{ collagen} \times 6.0 \text{ mg/ml} = 400 \mu\text{l} \times 4.0 \text{ mg/ml}$$

$$V \text{ collagen} = 266.7 \mu\text{l collagen}$$

Transfer this amount of stock collagen to the prechilled 1.5-ml tube using a positive-displacement pipettor and tip. **IMPORTANT NOTE:** Be sure to keep the tube of collagen on ice at all times.

3. Add 1/10th volume of 10 $\times$  DMEM and 10 $\times$  RB (40  $\mu$ l each), and mix well by pipetting up and down.
4. Centrifuge by pulsing for 10 s to remove any bubbles. It is okay to have bubbles when the collagen is mixed, as long as they are completely removed by centrifugation.
5. Add an initial 6  $\mu$ l of 1 N NaOH, mix well, and test the pH by putting a small drop on a pH strip and waiting 1-2 min for the pH to change. Adjust the pH until it is between 7.0 and 7.4 and the solution has a peach tint. The solution will turn bright red when NaOH is first added, but should turn orange/peach as the solution is mixed. If the color goes back to yellow, add 1 N NaOH in 1- $\mu$ l increments until it is peach color. If the pH exceeds 7.4, lower it using 1 N HCl. Keep track of the volumes of NaOH and HCl added, as the volume of DPBS will need to be adjusted accordingly. The required volume of NaOH will depend on the particular collagen preparation as well as the final desired concentration and volume of collagen.

6. Calculate the volume of DPBS ( $V_{DPBS}$ ) needed to reach the desired collagen concentration:

$$V_{DPBS} = V_{final} - V_{collagen} - V_{DMEM} - V_{RB} - V_{NaOH}$$

$$V_{DPBS} = 400 - 266.7 - 40 - 40 - V_{NaOH}$$

Add this volume of ice-cold DPBS to the neutralized collagen.

### **Embed spheroids in collagen gel**

7. Remove a 96-well U-bottom plate with spheroids from the incubator and examine all spheroids under an inverted microscope to ensure that they have formed tight, compact spheres rather than loose aggregates. Mark wells in which the cells are not spherical using a lab marker to avoid transferring them to the collagen gel.
8. Gently aspirate 100  $\mu$ l medium from one well, making sure to gently touch the pipette tip to the wall of the well without disturbing the spheroid. Add 100  $\mu$ l HBSS to the well to wash the spheroid.
9. Repeat two more times to ensure that the spheroid is adequately washed.
10. Cut off the tip of a 200- $\mu$ l pipette tip using a sharp, sterile razor blade. The blade can be sprayed with 70% ethanol to sterilize it.
11. Place an acid-washed and silanized MatTek dish on the cold tile for  $\sim$ 1 min to cool the bottom of the dish. Cooling the dish will keep the gel from starting to polymerize right away. The dish should not be left on the cold tile for more than 3-4 min, however, because it will start to accumulate condensation.

12. Gently aspirate the washed spheroid into the cut pipette tip, bring it to the very tip by expelling the medium between the spheroid and the tip, and then expel the spheroid into the neutralized collagen. This process minimizes the volume of medium transferred to the neutralized collagen. Multiple spheroids can be added to one MatTek dish. To keep the concentration of collagen consistent, an equal number of spheroids should be added to each dish.
13. Using the same cut tip, transfer 200  $\mu$ l neutralized collagen with spheroid(s) to the center of an activated MatTek dish. Spread the gel with the pipet tip so that it covers the entire bottom of the dish and check under an inverted microscope to ensure that there are no air bubbles at the edges of the glass circle.
14. Place the dish in a 37°C incubator for 30 min to allow the collagen gel to polymerize.
15. When the gel is opaque (indicating that it has polymerized), slowly add 2 ml warm medium to the dish by touching the pipette tip to the wall of the dish and slowly releasing the medium. Do not add less than 1 ml medium, as the medium can evaporate quickly in the incubator. Be careful not to disrupt the gel, because liquid can travel under the gel through small gaps, causing the collagen gel to pop off the coverslip.
16. Change the medium every 2 days by removing 2 ml and adding 2 ml fresh warm medium. Be very careful when aspirating medium from the dishes to avoid dislodging the collagen gel.

## **Alternative protocol: EMBEDDING OF TUMOR SPHEROIDS IN COLLAGEN GELS USING A SANDWICH METHOD**

For an easier approach to embedding the spheroids and controlling the distance at which the spheroids are situated above the glass bottom of the dish, one can sandwich the spheroid between two layers of collagen gel. Here, the bottom layer is fully polymerized, the spheroid is placed on top of this layer, and then the top layer is added over the spheroid and polymerized. It is important to note that some cell types can anomalously migrate along the horizontal plane between the two layers of collagen, rather than migrating outward in all dimensions through the gel. Other cell types, such as fibroblasts, will migrate outward easily into the collagen gels.

See Basic Protocol 2 for all materials.

1. Prepare neutralized collagen (see Basic Protocol 2, steps 1-6).
2. Place a MatTek dish on the cold tile for ~1 min to chill.
3. Place 60  $\mu$ l neutralized collagen in the center of the dish and spread it with the pipet tip so that it completely covers the glass surface.
4. Place the dish in the 37°C incubator for 30 min for the collagen to polymerize.
5. Check spheroids and wash three times with HBSS (see Basic Protocol 2, steps 7-9).
6. Using a cut 200- $\mu$ l pipette tip, gently aspirate a spheroid and place it in the center of the MatTek dish, on top of the polymerized collagen (see Basic Protocol 2, steps 10 and 12).

7. Pipette 140  $\mu$ l neutralized collagen onto the spheroid and tilt the dish to spread the collagen around the surface of the dish.
8. Return the dish to the incubator for 30 min for the collagen to polymerize.
9. Add warm medium to the dish and culture cells, changing the medium every 2 days (see Basic Protocol 2, steps 15-16).

## **Basic Protocol 3: FIXING AND IMMUNOSTAINING TUMOR SPHEROIDS EMBEDDED IN 3D COLLAGEN GELS**

One of the advantages of 3D spheroids embedded in a hydrogel is that the spheroid can be easily immunostained to study the individual or collective migration of its cells into its surrounding ECM. Staining and imaging of 3D spheroids make it possible to study multiple variables that could play a role in tumor invasion and metastasis.

### **Materials**

16% paraformaldehyde in aqueous solution (Electron Microscopy Sciences, VWR cat. no. 100503-914)

Dulbecco's PBS with calcium and magnesium (DPBS) chilled to 4°C (HyClone, cat. no. SH30264.02)

Spheroids embedded in collagen gel in MatTek dishes (Basic Protocol 2 or Alternate Protocol)

Triton X-100 (Sigma, cat. no. T9284)

Donkey serum (Sigma-Aldrich, cat. no. D9663)

Goat anti-collagen IV primary antibody (Millipore, cat. no. AB769)

Donkey anti-goat 647 immunofluorescent secondary antibody (Jackson ImmunoResearch, cat. no. 705-605-003)

Invitrogen DAPI (ThermoFisher Scientific, cat. no. D1306)

Invitrogen Alexa Fluor 488 Phalloidin (ThermoFisher Scientific, cat. no. A12370)

Rocker

Confocal microscope

## Protocol steps — *Step annotations:*

### Day 1

1. Before you start, prepare a 4% paraformaldehyde fixation solution by diluting the 16% paraformaldehyde solution in 1× DPBS, and warm the mixture up to 37°C. Make sure to handle paraformaldehyde in a fume hood. Prepare only the amount that you will use for each day's experiments and properly discard the rest in a chemical liquid waste container.
2. Remove the medium from each MatTek dish slowly by tilting the dish to one side, and, using a 1-ml pipette tip, carefully aspirate and remove the medium completely from the dish. Do not keep the dishes out too long at room temperature. After removal of the growth medium, immediately move to the next step. Cells can retract their protrusions if they are left out of 37°C for too long.
3. Immediately add the fixative solution from step 1 by slowly pipetting 2 ml down the wall of the MatTek dishes. Use a P1000 single-channel pipettor and 1000- $\mu$ l pipet tip. Leave for 1 hr at 37°C.
4. Aspirate the fixative solution and discard properly.
5. Wash with DPBS three times for 15 min each and leave the dishes on the rocker each time.
6. Freshly prepare a 0.5% Triton X-100 permeabilization solution in DPBS, add this to the MatTek dish, and leave on the dishes overnight in a 4°C cold room on the rocker.

7. Wash three times with DPBS. Each time gently rock the dishes using the rocker.
8. Prepare a blocking solution consisting of 5% donkey serum in DPBS, and add 500  $\mu$ l per well of the blocking solution in each of the MatTek dishes.
9. Prepare a primary antibody solution based on the manufacturer's recommended concentration. Here we prepare a 1:200 solution of collagen IV antibody in DPBS (optional: add 5% donkey serum to the antibody solution). Leave on a rocker for 4 hr at room temperature or at 4°C in cold room, overnight.
10. Aspirate and wash away unbound primary antibody with DPBS three times, 15 min each time on the rocker, at room temperature.
11. Prepare a secondary antibody solution by diluting donkey anti-goat 647 immunofluorescent secondary antibody at 1:200 dilution in DPBS. Also add DAPI (1:200 dilution) and phalloidin Alexa Fluor 488 (1:200 dilution) to this secondary antibody immunostaining solution. Leave the secondary antibody in the MatTek dishes for 4 hr at room temperature or overnight at 4°C in cold room.
12. Wash three times with DPBS. Each time gently rock the dishes using the rocker. After the last wash, put them in 1-2 ml of DPBS. You can store the dishes in 4°C for 3-4 days, but make sure to place them in a petri dish with the lid on, and parafilm the outside to keep the gels from drying out.
13. Image the spheroids using a confocal microscope.

## **REAGENTS AND SOLUTIONS**

*DMEM, 10X*

Dissolve 1 packet of powdered DMEM with phenol red (Sigma-Aldrich, cat. no. D2429) in 50 ml distilled water and stir at ~50°C until the powder goes into solution. While the solution is still warm, filter sterilize using a 0.2-µm filter (e.g., Steriflip, Millipore). Prepare aliquots of 1.0 ml and freeze using powdered dry ice. Store indefinitely at –20°C or up to 1 month at 4°C.

*NaOH, 1 N*

Dissolve 0.5 g NaOH pellets in 12.5 ml distilled water. Mix well, filter sterilize, and divide into 500-µl aliquots. Store indefinitely at –20°C.

*Reconstitution buffer (RB), 10×*

Measure out 2.2 g sodium bicarbonate and 4.8 g HEPES or 20 ml of 1 M HEPES stock solution for a 0.2 M final buffer concentration. Bring to 100 ml using distilled water and dissolve using a stir bar. Filter sterilize and prepare aliquots of 0.5 ml. Store indefinitely at –20°C or up to 1 month at 4°C.

*Supplemented DMEM (for MDA-231BO cells) Dulbecco's Modified Eagle Medium (DMEM; Gibco, cat. no. 11965-092) containing:*

10% fetal bovine serum (Life Technologies)

100 U/ml penicillin (Life Technologies)

100 µg/ml streptomycin (Life Technologies)

1% L-glutamine (Life Technologies)

Store up to expiration date on medium bottle at 4°C

*Supplemented DMEM/F12 (for MCF10A cells)*

DMEM/F12 medium (Life Technologies)

5% horse serum (Life Technologies)

20 ng/ml hEGF (Life Technologies)

100 U/ml penicillin (Life Technologies)

100 µg/ml streptomycin (Life Technologies)

## **Background Information**

Three-dimensional spheroid assays represent a recent approach to modeling tumors that has been shown to be superior to single-cell monolayer studies of tumor cells.

Although a 3D in vitro collagen hydrogel is not an exact replicate of original tissues such as mammary tumor tissue, it provides valuable insight into the morphological and signaling behavior of tumor cells during single-cell and collective cell migration in a 3D microenvironment. Migration studies in 3D are also more accurate because tumor cells tend to migrate outward in three dimensions in a more physiological ECM environment, instead of single-layer 2D migration on a stiff surface. Mouse models are valuable for modeling human disease, but they can be expensive, time consuming, and require

more effort than 3D spheroids, which can be formed as uniform spheroids that can be compared directly.

Other current 3D spheroid models do not possess an intact, well-formed basement membrane surrounding the spheroid. Most 3D models model the 3D microenvironment by mixing Matrigel and collagen I [55] or by using a mixture of agarose and Matrigel to form spheroids [56] —or they form a thicker and more diffuse layer around the spheroids that is not organized into a discrete, thin sheet of basement membrane [57]. With the protocols in this article, collagen IV and laminin are observed by immunostaining to be co-localized, with fibronectin decorating collagen I everywhere in the ECM hydrogel, surrounding the spheroid. We have used this technique to study single-cell and multicellular migration from a spheroid into 3D collagen.

### **Critical Parameters**

**Basic Protocol 1** After the addition of Matrigel, it is important to centrifuge the plate at room temperature. If you centrifuge at 4°C, the basement membrane may result in a “patchy” collagen IV surrounding the spheroid. Please note that the roundness of the spheroid also depends on the cell type itself. Some cells do not form perfect spheres even if you follow these exact steps.

**Basic Protocol 2** Do not skip the washing step with HBSS, since this will ensure that the spheroids do not have excess Matrigel around them that will subsequently create an

empty zone between the collagen I ECM and the spheroid. The cells in the spheroid will not migrate into such an empty area where the collagenous ECM is not immediately adjacent to the basement membrane and cells of the spheroid. Also make sure to perform the acid wash and activate MatTek dishes using silanization to ensure that the collagen gel will remain adherent to the bottom of the MatTek dish, and that cells will not drop to the bottom of the dish and will remain in the gel.

Basic Protocol 3 Be very careful when aspirating and releasing different solutions to the 3D gels, to ensure that you do not disturb the gel. Use a P1000 micropipetter and slowly aspirate and release medium by touching the tip to the wall of the MatTek dish, away from the 3D gel, to ensure that the gel does not pop off the glass coverslip.

### Understanding Results

In Basic Protocol 1, you should observe compact spheroids. The cells first form an aggregate because they are in a low-attachment plate, which results in the cells attaching to one another. If they have cell-cell adhesive capability, they will successfully aggregate in a lump of cells that may seem spherical, but which does not have a

defined edge and is not compacted. These cells prefer to attach to one another rather than to the low-attachment plate, and they form a spherical aggregate because that is the lowest energy state; nevertheless, they do not compact well. After the addition of Matrigel, the cells will form a more compact sphere, because they are confined within a tight basement membrane with laminin and collagen IV acting as a barrier to keep them

enclosed. Leaving the spheroids for 2 days will allow the sphere to become compacted and the cells to start multiplying. If you do not see this after following the troubleshooting steps in Table 1, cells may simply not be able to form spheroids due to a lack of sufficient cell-to-cell adhesion.

**Table 2.1.** Troubleshooting Guide for Generating Uniform Spheroids with an Intact, Thin, Single-Layer Basement Membrane, Embedding the Spheroids in Collagen Type I Gels, and Immunostaining  
 In Basic Protocol 2, the spheroids will be embedded in the collagen gel, and after 1 day they will start migrating out of the sphere and into the surrounding ECM, depending on the density of the collagen gel. In Basic Protocol 3, you can immunostain spheroids, and upon imaging with confocal microscopy, you may see that the spheroids can be bumpy and irregular, as shown in Figure 2.2.

Procedure	Problem	Possible cause	Solution
Uniform spheroid formation (Basic Protocol 1)	Spheroids did not form (cells are still in aggregates and there is no defined edge)	Did not centrifuge the plates after seeding and/or after adding Matrigel	Centrifuge plates the day after seeding and after adding Matrigel. Note that this is also dependent on the cell type, and some cells may form spheroids that are irregular in shape
Polymerizing collagen and embedding spheroid with basement membrane in collagen gels (Basic Protocol 2)	Matrigel is spread around the spheroid in an unorganized fashion	Did not wash the spheroid sufficiently with HBSS to remove excess Matrigel	Wash spheroids with HBSS and make sure you are removing more and more Matrigel/medium from the well with each wash
	Collagen gel	There were bubbles present at the edge of the gel at the junction	Always check under a
	pops off the coverslip	of the coverslip and the plastic MatTek dish	microscope after putting the neutralized collagen solution into the MatTek dish to ensure you have spread the gel uniformly over the coverslip with no holes or bubbles present
	Cells die in the gel	The gel has a low pH and it was not adjusted to neutral pH	Make sure to wait 1-2 min for the pH strip to show the correct pH and for the

<b>Procedure</b>	<b>Problem</b>	<b>Possible cause</b>	<b>Solution</b>
			gel mixture to turn a peach hue
Embedding the spheroids in collagen gels using the “sandwich” method (Alternate Protocol)	The cells migrate in between the two layers of gel	This can vary with different cells and their normal migration patterns in 3D. Some cells may find it easier to migrate through the two collagen layers instead of through the collagen fibers.	Follow Basic Protocol 1 to pre-mix the collagen gel and the spheroid in a tube before adding it into the MatTek dish
Fixing and immunostaining the 3D spheroid model (Basic Protocol 3)	There is no staining in the middle of the spheroid	The spheroid was not properly permeabilized	If permeabilized for only 2 hr, extend the permeabilization step for another 2-4 hr

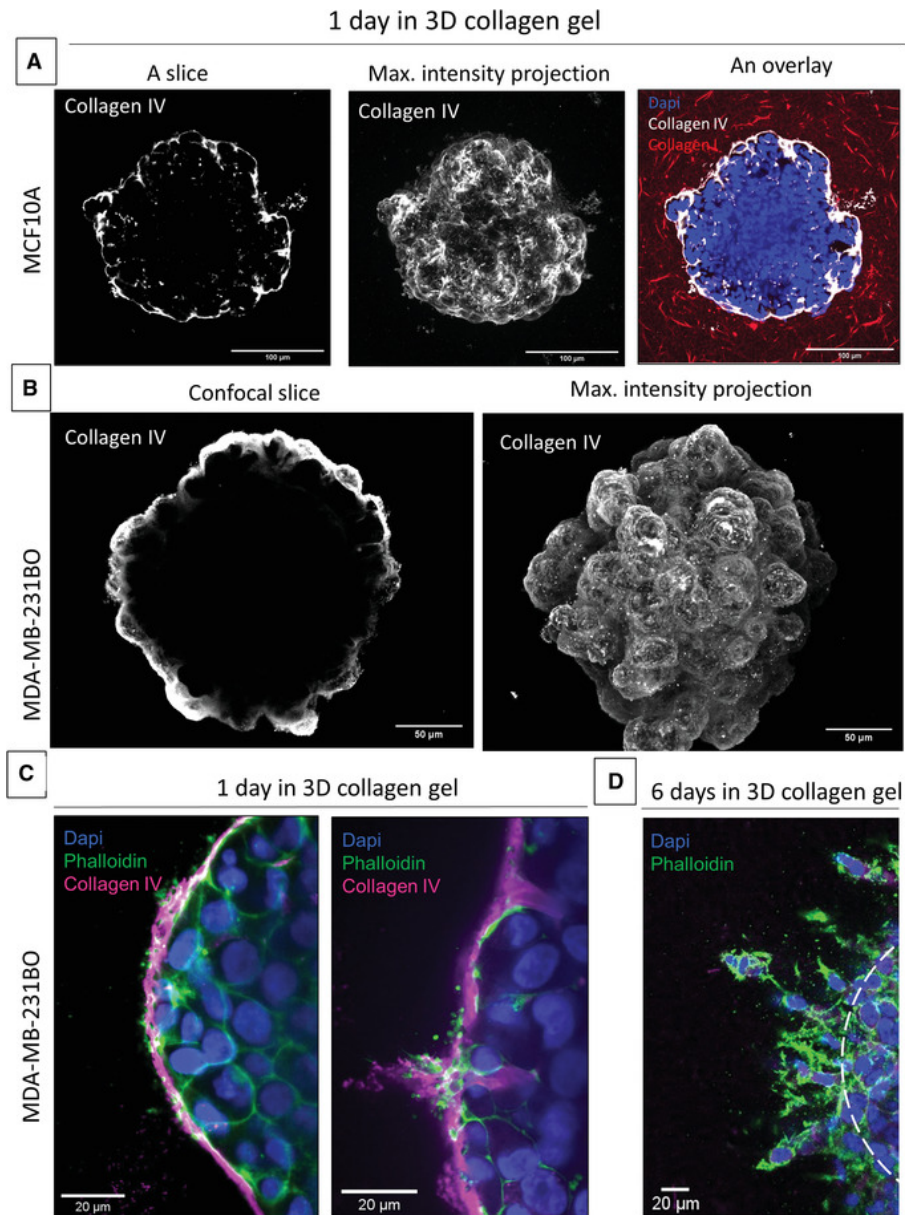


**Figure 2.2. Spheroids with encapsulating basement membrane in 3D collagen gels.**

(A) MCF10A spheroids confined by a basement membrane stained with collagen IV antibody and imaged using a confocal microscope. (B) MDA-231BO spheroid stained for collagen IV is shown as a confocal slice and a max-projection of the collagen IV surrounding the 3D spheroid. (C) High-resolution images of MDA-231BO spheroids with

an intact basement membrane before and after initial break through the basement membrane. **(D)** Six days after spheroids were incubated in 3D collagen gels, cells migrated into the 3D ECM. Note that the absence of a basement membrane or collagen IV staining is because the cells have broken out and migrated away from the initial spheroid, which is depicted by dashed lines.

## **Time Considerations**

Seeding cells for the spheroid assay takes 30 min. However, it requires approximately 5 days to generate spheroids with an encapsulating basement membrane (Basic Protocol 1). The time required for polymerizing collagen and embedding spheroids in collagen gels depends on the number of spheroids you are embedding. For about five spheroids in one MatTek dish, it will take approximately 30 min to complete, and then another 30 min to polymerize the gel in the incubator (Basic Protocol 2).

Fixing the spheroids and washing them takes about 2 hr. Permeabilizing the spheroids can be done at room temperature for 2 hr, or it can be done overnight to ensure that permeabilization occurs sufficiently deep in the spheroid. Blocking nonspecific sites in the spheroids takes 2 hr, and immunostaining the spheroids using primary and secondary antibodies requires 8 hr, or 2 days if left overnight, since diffusion of the antibodies into the interior of a chemically fixed spheroid is slow (Basic Protocol 3).

## CHAPTER 3:

### **Mechanisms of Basement Membrane Micro-Perforation during Cancer Cell**

#### **Invasion into a 3D Collagen Gel [58]**

#### **Preface**

This chapter contains work from our publication by MDPI publishing, by *Gels*, 2022, on which I am the first author of, entitled “*Mechanisms of Basement Membrane Micro-Perforations during Cancer Invasion into a 3D Collagen Gel*” [58]. I designed and carried out the experiments. Dr. Andrew Doyle helped with optimizing imaging analysis and providing general expertise in 3D imaging. Dr. Kenneth Yamada contributed to the general idea of the research, the direction of the project and helped extensively during manuscript editing and revision process. Oversight of this project was provided by my adviser, Dr. Kenneth M. Yamada. This manuscript was published in an OpenAccess journal which allows for the use of the content with proper citation and credit. No changes were made to the content of this chapter. This work is also a US Government work, therefore it is in the public domain in the USA.

## Introduction

The vast majority of cancer-associated deaths (about 90% of all cases) are caused by metastatic disease rather than primary tumors [2]. During epithelial cancer progression, epithelial cells lose their apical–basal polarity and become less organized, but they remain confined within a basement membrane (BM) barrier at the early cancer stage termed in situ carcinoma. At the second stage of tumor progression, cells penetrate through the basement membrane and invade the surrounding tissue. Cancer cells can then metastasize; they disseminate and migrate away from the primary tumor through the extracellular matrix (ECM), intravasate into blood vessels or the lymphatic system, and then extravasate and form secondary tumors at distant sites. Tumor metastasis is the leading cause of cancer-associated deaths; however, for carcinomas to metastasize they must first break through basement membrane barriers.

Basement membrane (BM) penetration is consequently the first important step in cancer invasion, ultimately leading to tumor metastasis and decreased patient survival. BM degradation also results in the release and activation of growth factors involved in angiogenesis, tumor invasion, and metastasis. Thus, it is important to identify the mechanisms involved in cancer cell breaching of the BM. BMs are thin, sheet-like structures comprising networks of laminin, collagen IV, perlecan, nidogen, and proteoglycans. Laminin can directly bind to cell surface receptors, such as  $\beta$ 1 integrin and dystroglycan, to self-assemble into a flat, dense sheet. Collagen IV then polymerizes to form a second covalently crosslinked network. These collagen IV polymers associate with the laminin polymers via nidogen/entactin crosslinks [12, 13, 59].

The BM serves as a structural layer that encapsulates epithelial and endothelial cells [12-14]. The BM is also a nanoporous structure. These submicron pores restrict cell movement and diffusion of large molecules through the BM, while allowing for permeability of small molecules. The size of BM pores varies depending on the tissue type, with the average pore size (the largest distance between fibers in three-dimensional space) of mammary epithelial BM measured to be only ~10 nm [12, 15]. During invasion, cancer cells penetrate the BM and migrate within the ECM toward the circulatory or the lymphatic system. Because a cell's nucleus is the largest organelle with a cross-sectional area ~10  $\mu\text{m}^2$ , cells must perforate the BM and expand these perforations sufficiently to allow the nucleus and cell body to traverse the BM and invade the surrounding microenvironment [12].

A well-known mechanism cells use to invade through the BM is local proteolysis of the BM and the surrounding stromal ECM. Localized basement membrane degradation requires membrane metalloproteases (MMPs), which also include the family of ADAMs (a disintegrin and metalloproteinase). MMPs are a family of zinc endopeptidases that cleave ECM molecules. ADAMs are enzymes that cleave growth factors, cytokine receptors, and adhesion molecules. MMPs are particularly important enzymes for ECM remodeling during wound healing, development, mammary gland involution, and angiogenesis. Cancer cells can form mechanosensitive actin-based protrusions called invadopodia that locally deliver proteases for ECM degradation and thereby enable penetration through the basement membrane [16-19]. A classic concept of BM invasion has proposed that cancer cells break through the BM barrier by chemical degradation using these proteases, particularly MMPs.

However, emerging evidence shows that besides proteases, physical mechanisms can also be involved in cell invasion. For example, numerous clinical trials treating patients with broad or more-specific MMP inhibitors failed to reduce mortality. Although this failure could have resulted from inadequate drug dosing or disease states too advanced to respond, recent findings suggest that cells may also be able to breach the BM barrier through physical mechanisms independently of proteases [12, 31-33]. In a *Caenorhabditis elegans* (*C. elegans*) developmental model of BM invasion, cells can gradually breach the BM without proteases through force application to physically displace the BM, expanding the hole to permit slower but eventual invasion [14]. However, whether human cancer cells can similarly disrupt intact BMs without using any protease activity is not yet known.

Some of the main limitations for studying early events in cell invasion and BM breaching is that invasion is rare and occurs deep in the body, so being able to catch tumors undergoing the initial steps of cancer invasion is challenging. Moreover, tumors excised from humans or animals often lack a continuous BM [60], making it difficult to study the initial cell–ECM interactions at the BM interface. In contrast, we previously created an in vitro model of invasion that uses confocal microscopy to visualize human cancer cells as they perforate the BM for studies of the mechanisms of BM perforation and hole expansion during cancer invasion [41].

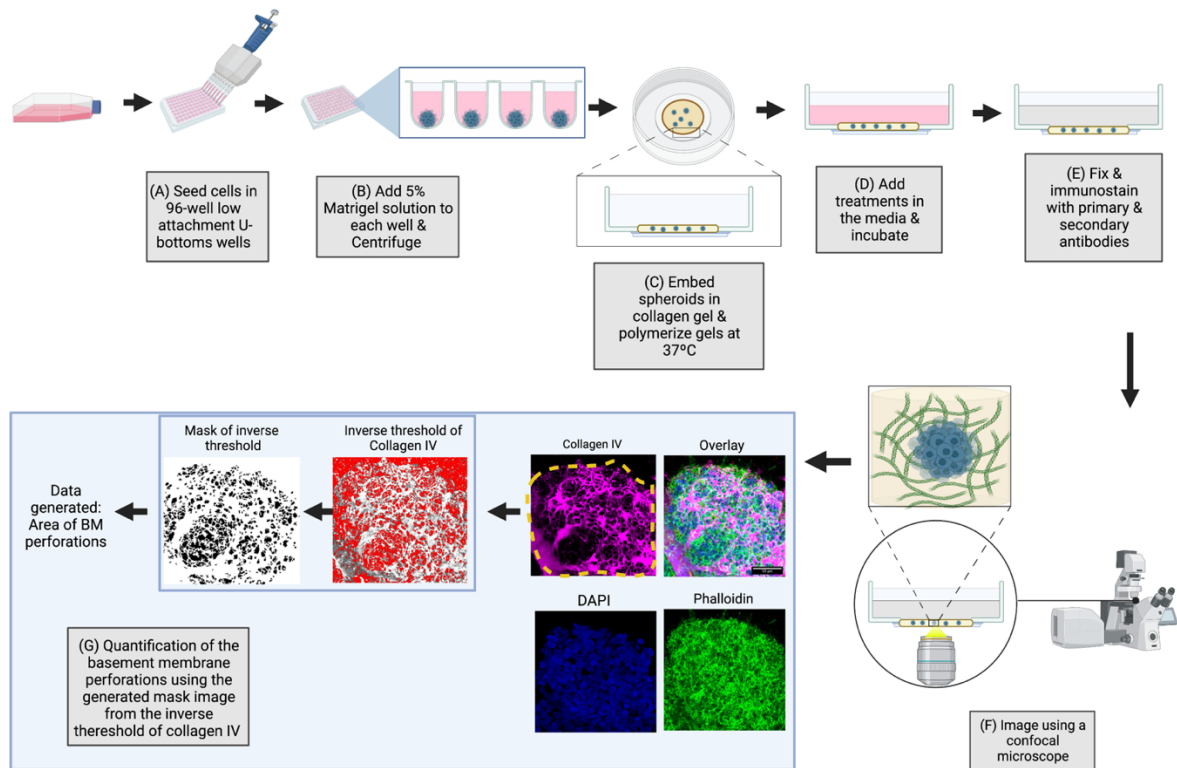
Recent studies on BM breaching have tended to focus on individual cells in 3D collagen gels, *C. elegans* models, or synthetic 3D cell cultures to characterize invasion and migration. Previous studies have also examined the contributions of myoepithelial, stromal, and immune cells to BM perforation and cancer cell invasion [36, 37, 61, 62].

Here, in this study, we focused on the contributions of cancer cells themselves to BM penetration and invasion with an emphasis on establishing the cellular mechanisms. We report that during early human cancer cell invasion from cancer spheroids, the BM was initially perforated by cells using actin polymerization, protease degradation, and a modest contribution from actomyosin contractility.

## Results and Discussion

### *Overview of the 3D-Spheroid Model*

To investigate the mechanisms of human cancer cell breaching through the BM, we used our three-dimensional in vitro invasion model (scheme 3.1). The spheroids were first encapsulated within a BM, and then the BM-containing spheroids were embedded in 3D collagen gels. Over the next ~18 to 36 h, the cells migrated from the spheroid and into the collagen microenvironment through collective cell migration, often in a “sunray” or “sunburst” pattern comprising narrow columns of cells (Figure 3.1).



**Scheme 3.1. Schematic illustration of the protocol for generating cancer cell spheroids encapsulated in a basement membrane and embedded in a 3D collagen gel for invasion assays.**

(A) In the spheroid generation process, cells were seeded in a 96-well, low attachment V- or U-bottom dish. To form aggregates, after 8 h the plate was centrifuged at 300 RPM for 5 min. (B) To form spheroids with an intact basement membrane, a dilute solution of Matrigel was added to the spheroids at a final concentration of 5% Matrigel per well. The plate was centrifuged again at 300 RPM for 5 min. (C) After the plate had incubated for several days at 37 °C, the spheroids were embedded in neutralized collagen gels at 4 mg/mL gel concentration, and the gel was polymerized at 37 °C for 1 h. (D) Culture medium and any treatments (if applicable) were added to the spheroids in the dishes. (E)

At the appropriate time, spheroids were then fixed with 4% paraformaldehyde and immunostained with primary (collagen IV) and secondary antibodies accompanied by DAPI (nuclear stain) and phalloidin (F-actin stain). **(F)** Spheroids were imaged via confocal microscopy. **(G)** For basement membrane perforation quantification, maximum intensity projections of the collagen IV channel were generated, and a region of interest was drawn around the boundary of the BM to delineate the total spheroid area (yellow dashed line). From this ROI, we generated an inverse threshold image and subsequently a masked version of it, from which we calculated the area of each perforation within the ROI, as well as the area of the ROI.

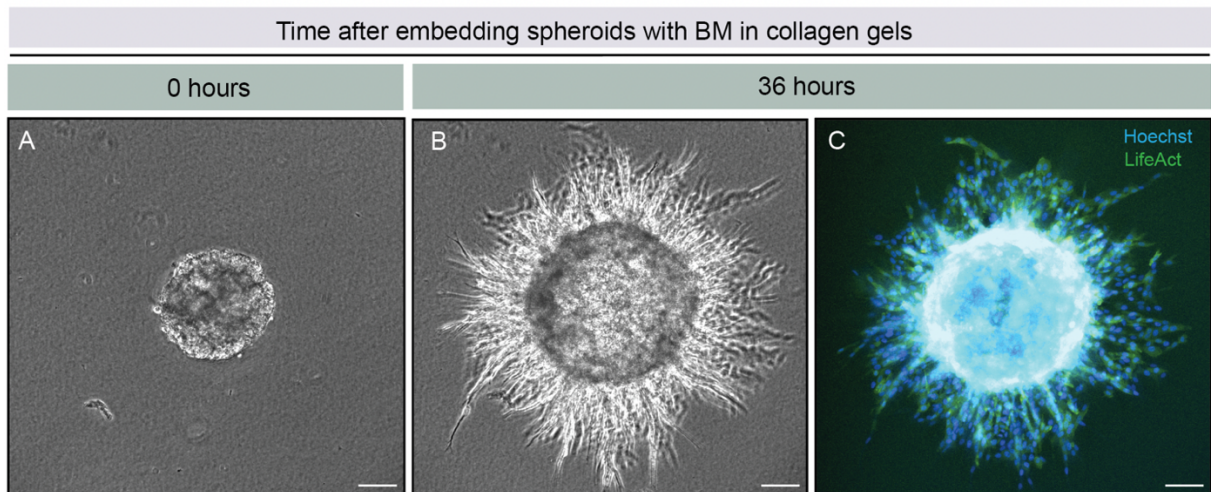


**Figure 3.2. Spheroid invasion through the basement membrane and into a collagen gel.**

(**A**) Spheroid after embedding in a collagen gel and polymerizing the gel (time 0 h) compared to a spheroid after 36 h (**B,C**). Cancer cells in the spheroid invaded into the surrounding collagen gel and exhibited a “sunburst” phenotype which entails a trail of cells outward from the main spheroid body. We noted that, besides the outward invasion of cancer cells into the collagen gel, the spheroid expanded at 36 h due to ongoing cell proliferation. Scale bars: (**A–C**), 100  $\mu\text{m}$ .

***BM Encapsulated Spheroids before Invasion and Became Extensively Perforated in Our Three-Dimensional In Vitro Invasion Assay***

We first evaluated whether any microscopic holes existed in the BM prior to invasion by fixing spheroids prior to embedding in collagen I gels that were 20 mm in diameter and approximately 500  $\mu\text{m}$  thick. As we have shown previously [41], immunostaining and confocal microscopy for collagen IV revealed a relatively continuous sheet of varying thickness (approximately 0.2–5  $\mu\text{m}$  thick) surrounding the spheroid (including the peripheral cells of the spheroid) with few apparent holes (Figure 3.2A). After 24 h incubation in culture media, followed by fixing and immunostaining for collagen IV, we observed perforations in the BM with varying sizes ranging from submicron to holes that could fit multiple nuclei (Figure 3.2B—magnified images). As predicted, we also observed many nuclei outside of the perforated BM suggesting that many cells invaded through the BM. The observation of holes larger than the diameter of a nucleus (the largest organelle of a cell) contrasted with previous characterizations of non-cancerous embryonic tissues by our laboratory in which micro-perforated BM surrounded expanding embryonic epithelia of lung, kidney, and salivary glands during branching morphogenesis [11]. These microscopic holes in embryonic BM were smaller than the diameter of the underlying epithelial cells and only contained the cytoplasmic extensions of the epithelial cells that protruded through these holes, but the cell bodies did not cross the BM. Recently, another laboratory observed similar micro-perforations in the BM that encases the embryo during mouse embryogenesis [38]. In contrast with the perforations during embryonic branching morphogenesis and mouse embryogenesis, the assay with cancer spheroids revealed

cells within larger BM perforations with many cells that penetrated through the BM and traversed into the collagen gel (Figure 3.2B). In the magnified images of Figure 3.2B we observed some holes containing one or more cells traversing the BM. The collective cell migration mode, showing the “sunray” phenotype of radially oriented columns of invading cells, demonstrated that although cells could perforate and traverse many holes in the BM, they often trailed behind leader cells in this collagen gel, which may have provided a path of least resistance. Laminin also was present and co-immunolocalized with collagen IV staining in the BM (Figure 3.2C). Consequently, although the source of BM we used in this assay was a diluted, soluble basement membrane extract (Matrigel), the spheroid cells could assemble overlapping the collagen IV and laminin networks that fully encapsulated the spheroid before any subsequent formation of perforations and invasion.

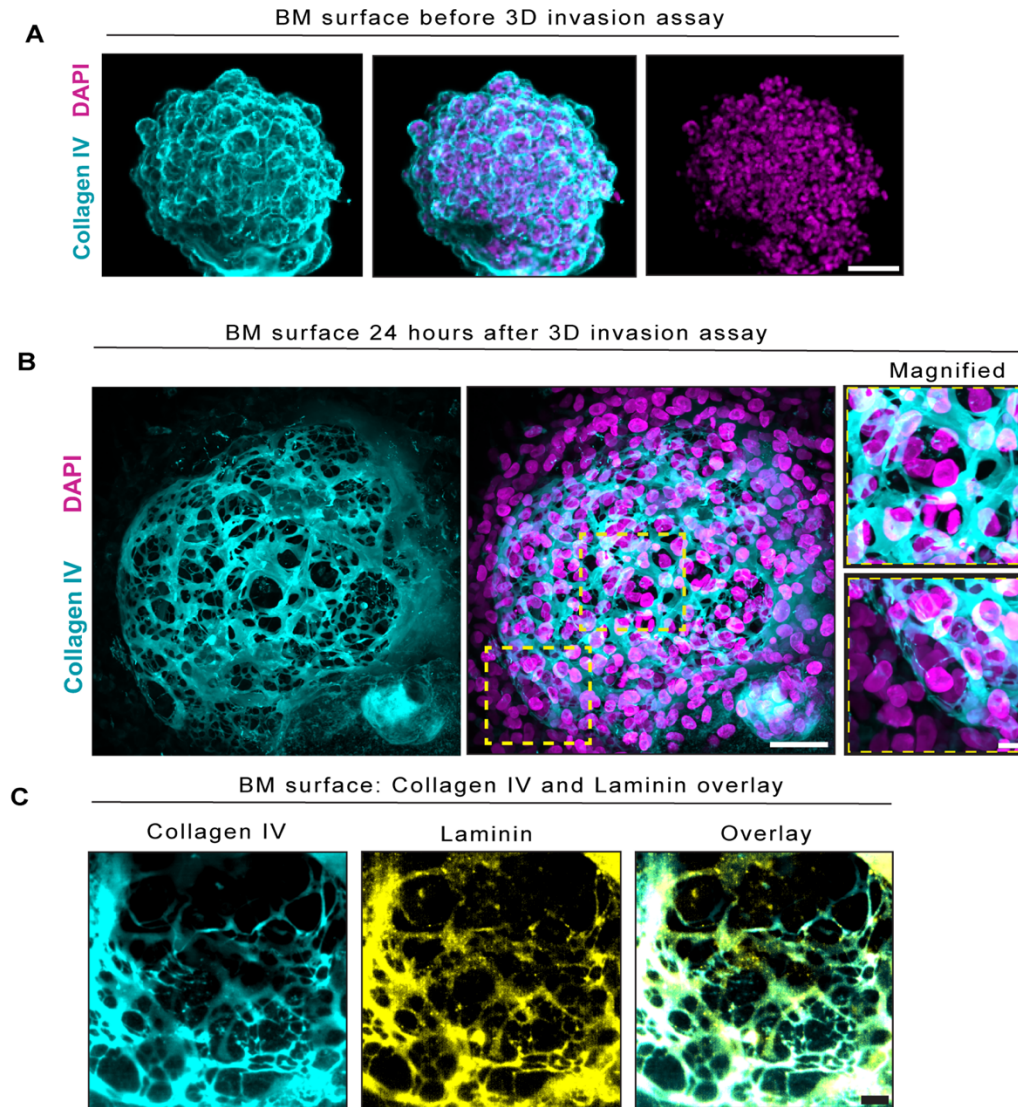


**Figure 3.2. Large perforations in the basement membrane appeared as cancer cells invaded.**

(A) Images show a spheroid with a basement membrane visualized by immunostaining for anti-collagen IV antibody and DAPI (staining for nuclei) before it was embedded in collagen gel. We observed no apparent holes in the basement membrane before the invasion assay. (B) 24 h after the spheroids were embedded in collagen gels, large holes

were visible with collagen IV immunostaining (cyan) of the basement membrane (upper inset). DAPI staining denoting cell nuclei (magenta) demonstrated many cells outside of the basement membrane (lower inset). **(C)** Immunolocalization of collagen IV (cyan) and laminin (yellow) staining in the in vitro basement membrane. These figures are representatives of at least 3 independent experiments, each including at least 3 spheroids per experiment, all of which showed similar results. Scale bars: **(A,B)**, 100  $\mu\text{m}$ ; Inset of **(B,C)**, 10  $\mu\text{m}$ .

### ***BM Perforations Expanded over Time as Cancer Cells Initiated Invasion through the BM***

To examine whether the BM perforations expand over time and whether their expansion correlates with cell invasion through the BM, we quantified the areas of the individual perforations in the BM over time (Figure 3.3B). To understand the progression of the BM perforation process, we embedded spheroids in a collagen I gel, and after polymerization (1 h at 37 °C), fixed samples at 0 (1 h after polymerization), 8, 18, and 24 h. Small perforations in the BM appeared by time 0 after gel polymerization (Figure 3.3A—time 0-h). By 8 h after spheroid embedding in collagen gels, the BM showed a significant increase in the hole number (~2.7-fold increase), yet with perforation areas similar to the 0 h timepoint, but with no visible invasion across the BM (Figure 3.3B,C). The absence of cellular invasion at 8 h (mean perforation area:  $6.9 \mu\text{m}^2 \pm 8.1 \text{ SD}$ ) was consistent with the finding that the average nuclear cross-sectional area was  $10.2 \mu\text{m}^2 \pm 0.3 \text{ SD}$ , i.e., often too large to pass through the perforation at 8 h, which thus likely prevented effective cell invasion through the BM (Figure 3.3B). Invasion was evident at 18 h when the perforation size exceeded the nuclear cross-sectional area (Figure 3.3A,B). However, the perforation number did not change between 8 h (pre-invasion) to 18 h (after invasion), suggesting that the subcellular holes were not simply merging to make larger holes but rather expanding over time (Figure 3.3C). Interestingly at 24 h, while more cells were observed trailing behind the leader cells breaching the BM and invading further out into the 3D collagen gel, there was no change in the hole size or number (Figure 3.3C), suggesting that the cells did not need to generate more or expand existing holes and simply followed along paths of least resistance.

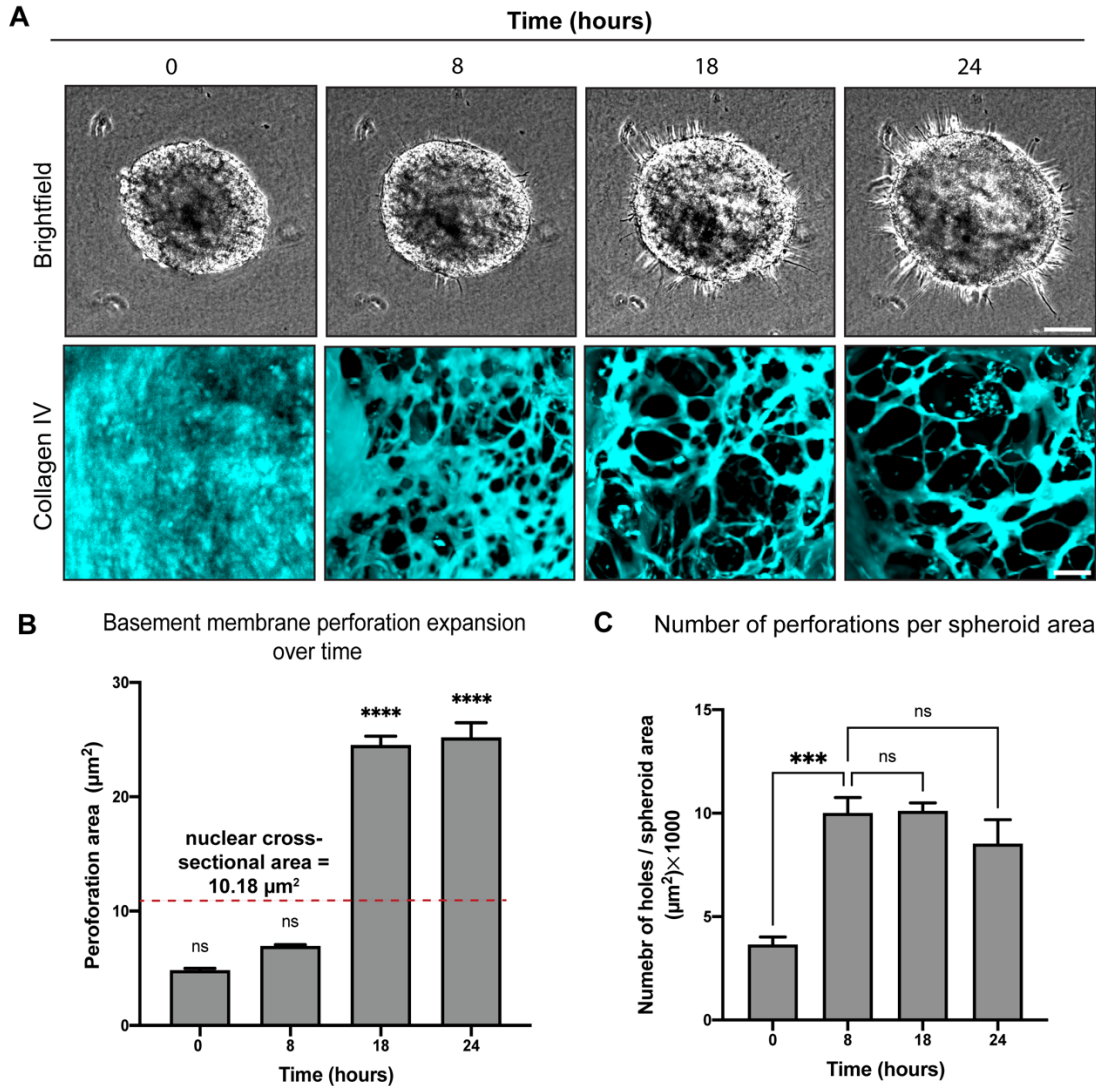


**Figure 3.3. Basement membrane perforation over time.**

(A) Brightfield images of a spheroid from a time-lapse video spanning 24 h (upper images) and basement membrane perforations from the same time points depicted by collagen IV staining (lower images). (B) Quantification of the average areas of individual basement membrane holes ( $\pm$  SEM) at each of the corresponding time points (lower images). Dashed line on the graph indicates the mean nuclear cross-sectional area of MDA-MB-231BO cancer cells. (C) Quantification of the number of holes per spheroid area. \*\*\*\*  $p < 0.0001$  \*\*\*  $p < 0.0003$ . These graphs are based on pooled data from at least 3 independent

experiments each including at least 3 spheroids per experiment, all of which showed similar results. Scale bars: **(A)**, top row, 100  $\mu\text{m}$ ; **(A)**, bottom row, 10  $\mu\text{m}$ .

### ***Protease Activity Played a More Important Role than Actomyosin Contractility in Perforating the BM during Cancer Cell Invasion***

Developmental models of invasion have revealed that besides proteases, other mechanisms can play a role in the formation and expansion of perforations [11, 12]. One mechanism is actomyosin contractility [11]. Previously, our laboratory had discovered that during embryonic salivary gland branching morphogenesis, epithelial expansion depends on both proteases for BM distensibility and perforation and actomyosin contractility for expanding BM perforations and remodeling the matrix, with these two processes apparently synergizing [11].

To determine the mechanisms of perforation expansion by cancer spheroids, we first used small molecule inhibitors to disrupt proteolysis and actomyosin contractility. Because the mean perforation cross-sectional area exceeded the nuclear cross-sectional area of cells at 18 h, we chose this time point for assaying the inhibitor treatments. After treating spheroids with a variety of MMP protease inhibitors (BB94, GM6001, TIMP2, and TIMP3) for 18 h, we observed substantial reductions in the size of the holes accompanied by increased fluorescence intensity of collagen IV immunostaining, suggesting an apparent thickening (inhibition of turnover; data not shown) of the BM (Figure 3.4A,B). This suppression of perforation expansion was accompanied by decreased invasion of cancer cells (Figure 3.4D). Specifically, batimastat (BB94) produced one of the most dramatic reductions in the sizes of the holes with a 63% reduction compared to control, while GM6001, a less broad-range inhibitor, still substantially inhibited perforation size by 56% (Figure 3.4B) and significantly reduced cell invasion (Figure 3.4D). The natural protease inhibitor TIMP2 (tissue inhibitor of metalloproteinases-2) that inhibits a subset

of MMPs had the most dramatic effect on the perforation cross-sectional area, reducing it by 68% and inhibiting cell invasion compared to its control (Figure 3.4C). TIMP3, which inhibits several MMPs and ADAMs (a disintegrin and metalloprotease), had a lower (55% reduction) but significant effect on inhibition of the perforation area (Figure 3.4C). Inhibition of actomyosin contractility with blebbistatin (a specific myosin II ATPase inhibitor) had modest effects on the BM perforation areas (15% reduction) compared to the major effects of protease inhibition (Figure 3.4B). These results are consistent with numerous previous studies implicating proteases in BM breaching. However, while contractility has been reported to aid in perforating the BM during breaching, our findings indicate that proteolysis, and not actomyosin contractility, appeared to be most important for perforation expansion to permit cancer cells to invade in this human spheroid system. To test for potential cooperativity between proteolysis and actomyosin contractility during hole formation by spheroid cancer cells, we treated the spheroids with a combination of BB94 and blebbistatin or with GM6001 plus blebbistatin, which reduced the perforation area by 47% and 38%, respectively, compared to their controls (Figure 3.4A—bottom row and Figure 3.4B). Although these combined treatments resulted in significant reductions in perforation size and cell invasion, in both cases, this reduction was not quite as dramatic as even BB94 or GM6001 alone. That is, there was clearly no evidence for cooperation between proteolysis and actomyosin contractility in this cancer cell spheroid invasion model. These findings contrast with the results in a developmental model of BM perforation where treatment of embryonic salivary glands [11] with similar inhibitor combinations had a more rapid and dramatic effect on BM perforation than either treatment alone. In a *C. elegans* model for invasion, actomyosin contractility could even

eventually drive BM breaching in the absence of protease activity [5]. Our results, differing from developmental models, suggested that there could be other mechanisms contributing to hole formation in the BM during the invasion of cancer cells.

To test for potential cooperativity between proteolysis and actomyosin contractility during hole formation by spheroid cancer cells, we treated the spheroids with a combination of BB94 and blebbistatin or with GM6001 plus blebbistatin, which reduced the perforation area by 47% and 38%, respectively, compared to their controls (Figure 3.4A—bottom row and Figure 3.4B). Although these combined treatments resulted in significant reductions in perforation size and cell invasion, in both cases, this reduction was not quite as dramatic as even BB94 or GM6001 alone. That is, there was clearly no evidence for cooperation between proteolysis and actomyosin contractility in this cancer cell spheroid invasion model. These findings contrast with the results in a developmental model of BM perforation where treatment of embryonic salivary glands [11] with similar inhibitor combinations had a more rapid and dramatic effect on BM perforation than either treatment alone. In a *C. elegans* model for invasion, actomyosin contractility could even eventually drive BM breaching in the absence of protease activity [5]. Our results, differing from developmental models, suggested that there could be other mechanisms contributing to hole formation in the BM during the invasion of cancer cells.

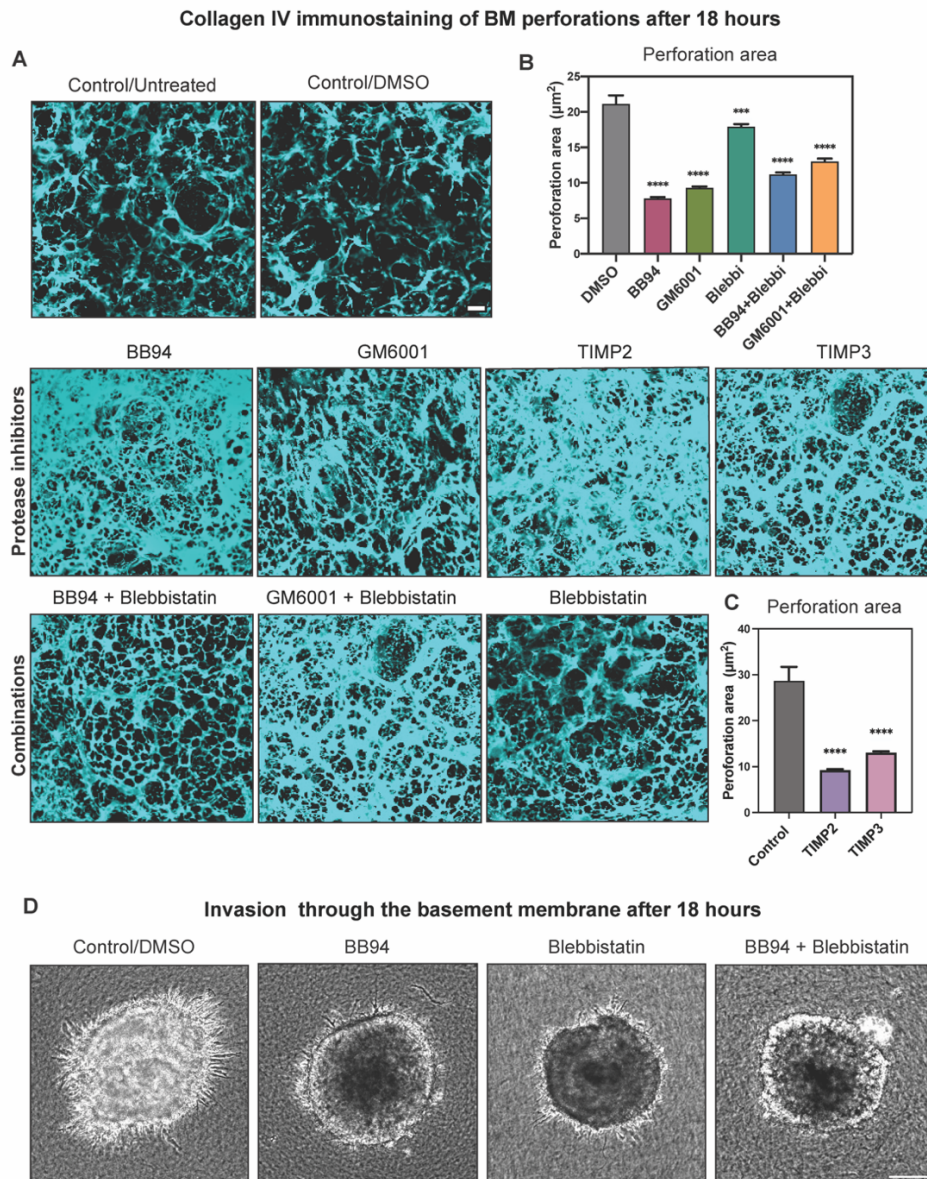


**Figure 3.4. Contributions of proteolysis and myosin II contractility to basement membrane perforation.**

(A) Maximum intensity projection images of the basement membrane surrounding the spheroid after 18 h treatment with the following protease inhibitors or combinations of inhibitors: control (untreated), control (DMSO), BB94, GM6001, TIMP2, TIMP3,

blebbistatin, BB94 + blebbistatin, or GM6001 + blebbistatin. **(B)** Quantification of basement membrane perforation areas after treatment with the indicated small molecule inhibitors during 18 h cancer cell invasion. **(C)** Quantification of perforation area in comparisons of TIMP2 and TIMP3 versus control. **(D)** Brightfield images of spheroids shown in panel A treated with small-molecule inhibitors of proteases (BB94), myosin II (blebbistatin), or a combination of BB94 and blebbistatin. \*\*\*\*  $p < 0.0001$ ; \*\*\* $p < 0.0007$ . These graphs and images are based on pooled data from at least 3 independent experiments, each including at least 3 spheroids per experiment, all of which showed similar results. Scale bars: **(A)**, 10  $\mu\text{m}$ ; **(D)**, 100  $\mu\text{m}$ .

### ***Actin Polymerization Dramatically Affected Hole Formation and Acted as a Third Mechanism Contributing to Perforation of the BM***

A classical cytoskeletal mechanism for the formation of cellular protrusions is actin polymerization. In the *C. elegans* model of BM invasion, cells can initially perforate the BM using actin-based invadopodia and actomyosin contractility with a subsequent large cellular protrusion to penetrate through the BM without the use of proteases by applying force to deform the BM, thereby enabling a slower but eventual invasion [12, 14]. However, a role for actin polymerization in collective cancer cell invasion through a BM has not been fully explored. To test for a role for this mechanism, we inhibited actin polymerization using either cytochalasin D or latrunculin A. Both small molecule inhibitors had dramatic inhibitory effects on hole formation and expansion (Figure 3.5A,B). To inhibit the F-actin nucleating complex ARP2/3, we used the small molecule inhibitor CK666, which provided evidence that actin branching polymerization played a role in expansion of perforations in the BM (Figure 3.5A—bottom left panel). Turning to the effects of these inhibitors on the process of invasion, inhibiting actin polymerization and perforation expansion completely inhibited cancer cell invasion through the BM (Figure 3.5C). The Rho-kinase inhibitor Y-27632 also significantly decreased the perforation size in the BM (Figure 3.5A,B) and decreased cell invasion (Figure 3.5C). Y-27632 can inhibit actin polymerization through Diaphanous-related formins (Dia1–3) and cofilin [63, 64], which could explain why it inhibited the expansion of perforations more than inhibiting actomyosin contractility using blebbistatin (Figure 3.4).

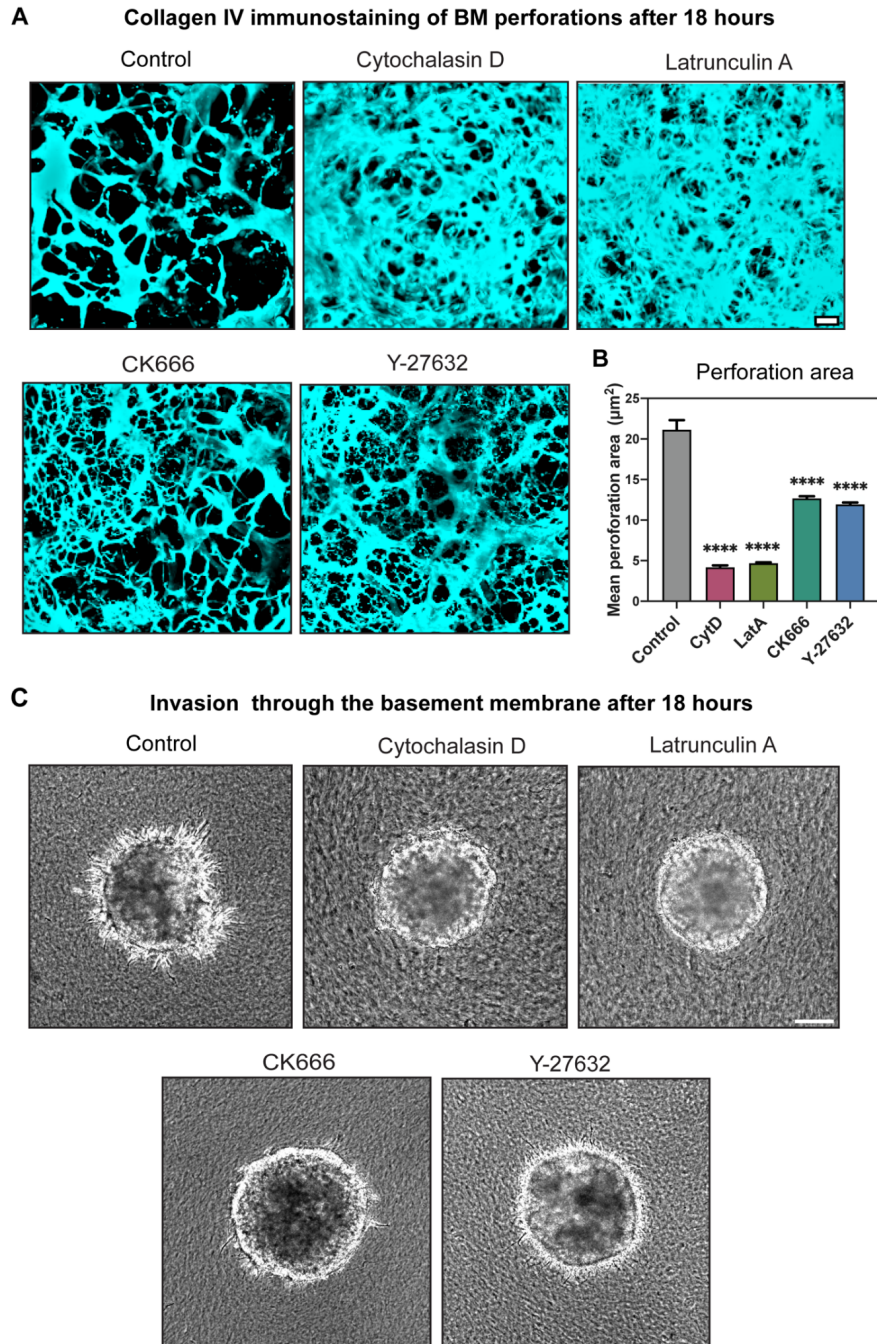


**Figure 3.5. Contribution of actin polymerization to basement membrane perforation during collective cancer cell invasion.**

(A) Confocal immunofluorescence images of the basement membrane (anti-collagen IV antibody) after treatment with the following inhibitors: cytochalasin D (actin), latrunculin A (actin), CK-666 (ARP2/3), or Y-27632 (ROCK). (B) Quantification of basement membrane

perforation areas for each treatment at 18 h. **(C)** Brightfield images of the spheroids after each treatment, showing the effects of the inhibitors on cell invasion. \*\*\*\*  $p < 0.0001$ . These graphs and images are based on pooled data from at least 3 independent experiments, each including at least 3 spheroids per experiment, all of which showed similar results. Scale bars: **(A)**, 10  $\mu\text{m}$ ; **(C)**, 100  $\mu\text{m}$ .

### ***Comparisons with Other Cell Types Confirmed Findings for Another Metastatic Cell but Not for a Non-Metastatic Cell Line***

We tested a second metastatic cell line to determine whether its spheroids would also generate large BM holes in our in vitro cancer invasion assay. We used 4T1 cells, a murine mammary tumor line that is generally very aggressive. After generating 4T1 spheroids with a BM and embedding them in collagen gels, we observed that, at 24 h, these cancer cells similarly invaded through the BM and out into the surrounding collagen gel (Figure 3.6A). Additionally, immunofluorescence anti-collagen IV staining revealed that there were large holes in the BM similar to those formed by the MDA-MB-231BO cell line (Figure 3.6D). We tested several inhibitors for their ability to suppress 4T1 invasion that targeted MMPs, contractility, and actin polymerization and found that they similarly suppressed invasion compared to controls (Figure 3.6A–C,E–F). Overall, these results confirmed findings with the main cell line we had tested.

To determine whether invasion and BM holes would be generated by a non-metastatic human cell line, we used MCF10A cells in our invasion assay. Their spheroids were similarly encapsulated in a BM and were embedded in collagen gels. After 24 h, however, we found no apparent holes in the BM or outward invasion into the collagen gel (Figure 3.7A).

In summary, we found that a metastatic cancer line from another species mimicked the BM perforation and outward invasion into collagen gels from spheroids, whereas a non-metastatic human cell line did not. We note that one limitation of this study is that we did not test large numbers of other types of cancer cells to determine whether the mechanisms we described for forming and expanding BM perforations were displayed by

all cancers. A second limitation is that these are obviously in vitro model studies, so examining these mechanisms in vivo would be valuable if future technical advances could make it feasible to evaluate the mechanisms of these initial steps of BM breaching by human cancer cells in living tissues.

4T1 spheroids with a basement membrane after 24 hours

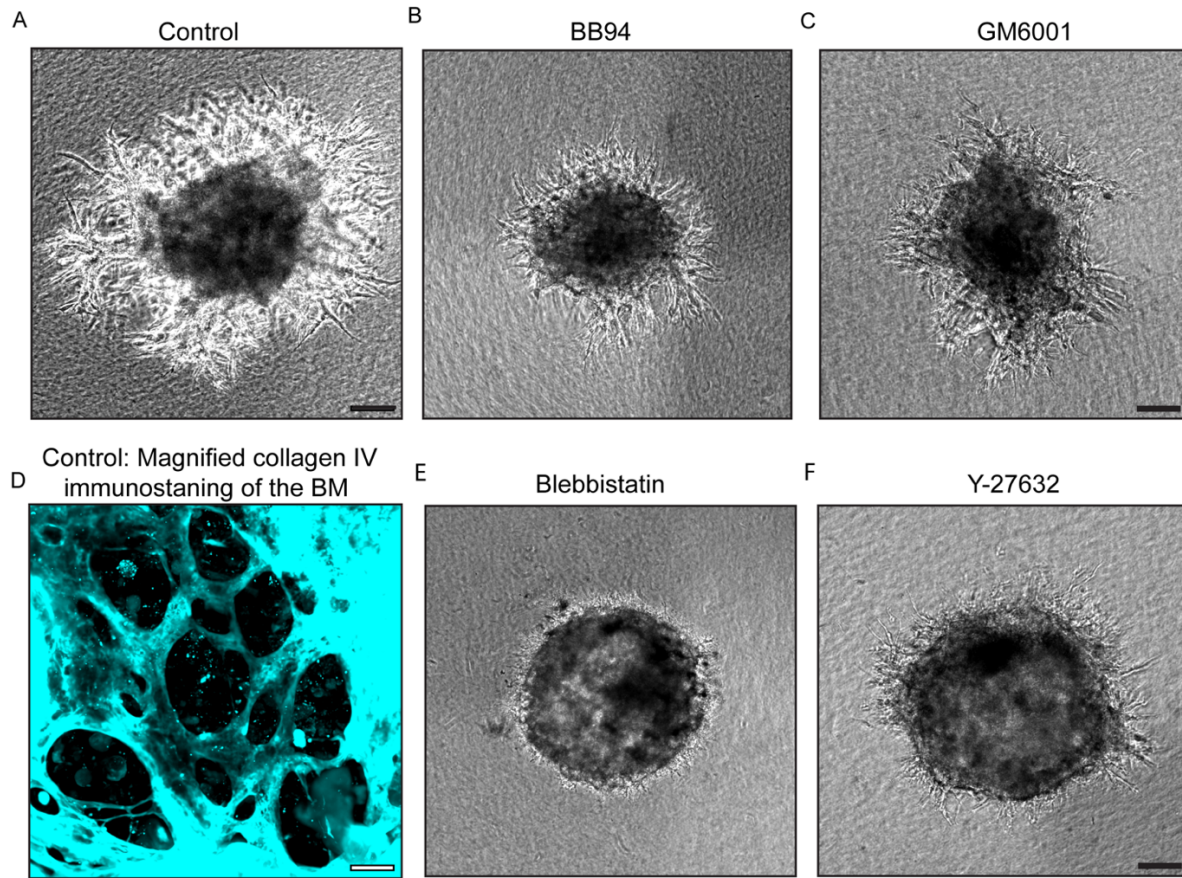


**Figure 3.6. 4T1 spheroids show perforations in the basement membrane after 24 hours.**

(A) spheroids from a murine tumor cell line, 4T1, invade into the collagen gel after 24 hours (B-C). Protease and MMP inhibition with BB94 and GM6001 decrease cell invasion similar to those for MDA-MB-231BO cell line. (D-E) Inhibition of myosin II, ROCK or actin polymerization also reduces cell invasion compared to control (D-E). Perforations are seen in the basement membrane of 4T1 control spheroids 24 hours after invasion, similar to MDA-MB-231BO cell line. Scale bars: A-C & E-F, 100  $\mu\text{m}$ ; D, 20  $\mu\text{m}$ .

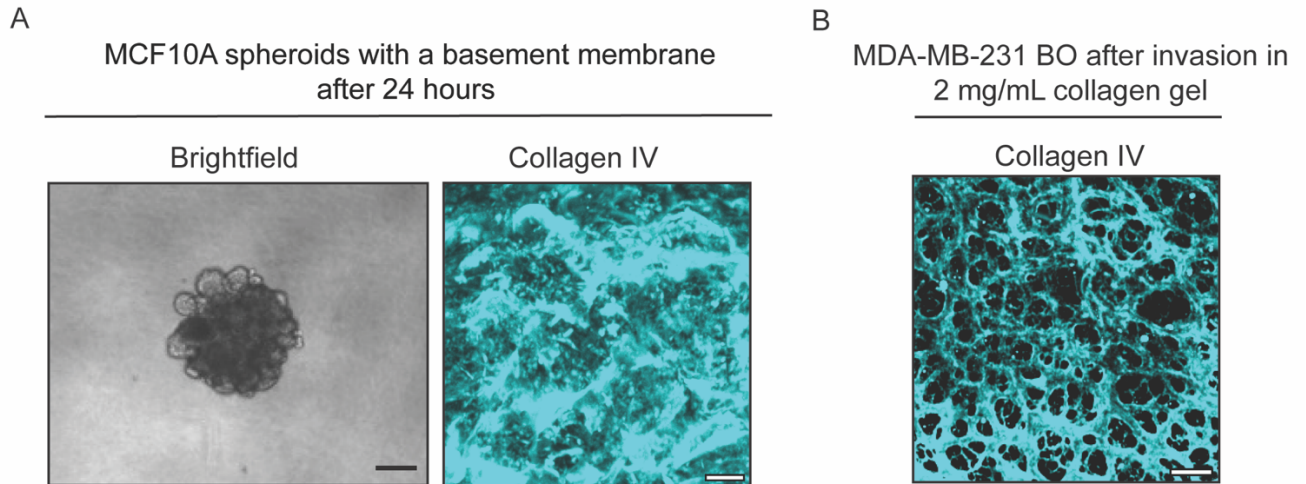


**Figure 3.7. A non-metastatic cell line does not generate large holes or invade into collagen gels.**

(A) Normal-like mammary cell line, MCF10A, formed a spheroid with a basement membrane and after embedding in collagen gel for 24 hours, the cells did not invade and they are no apparent large-holes in the basement membrane. (B) MDA-MB231BO spheroids embedded in 2 mg/mL collagen gels form holes in the basement membrane after 8 hours of invasion assay, similar to MDA-MB-231BO embedded in 4 mg/mL collagen gel. Scale bars: A (left panel), 100  $\mu\text{m}$ ; A (right panel), 10  $\mu\text{m}$ ; B, 10  $\mu\text{m}$ .

## Conclusions

Taken together, our results indicate that there were multiple mechanisms contributing to cancer cell BM breaching. They included actin polymerization and proteolysis, with a lesser contribution from actomyosin contractility. It was originally hypothesized that chemical degradation by proteases is key to BM penetration and invasion. From the developmental models, our understanding of invasion expanded to include the contribution of myosin contractility to invasion. The current study focusing on human cancer cell spheroids in a 3D in vitro model of invasion further confirmed that tumor cells could use proteases for initial perforation of the BM. However, we found that the sizes of the perforations were important: when they were smaller than the diameter of a cell, there was minimal invasion, but once the perforation area expanded beyond this size threshold needed to allow cells to traverse the BM, the cancer cells invaded outward. Importantly, we also identified a key role for actin polymerization in order for cell protrusions to expand the BM perforation areas to be able to invade, with a much lower requirement for actomyosin contractility than had been predicted from embryological models. Consequently, the dual functions of MMP-based proteolysis and cytoskeletal actin polymerization were crucial for effective BM perforation and human tumor cell breaching of the BM barrier to mediate cancer invasion.

## **CHAPTER 4:**

### **Long Prehensile Protrusions Displace Collagen and Pull Cells through the Basement Membrane during Cancer Invasion**

#### **Preface**

This chapter contains work from our collaborative project. I designed and carried out the experiments, live cell and confocal imaging, and analysis. Dr. Andrew Doyle helped the ablation experiment and with optimizing imaging analysis. Dr. Kenneth Yamada contributed to the general idea of the research, the direction of the project and helped extensively during the editing process of the chapter. Oversight of this project was provided by my adviser, Dr. Kenneth M. Yamada.

## Introduction

Cancer metastasis is the major cause of mortality in many cancer-related deaths. Metastasis occurs through a multi-step process of cancer cell invasion, dissemination of cells into the extracellular matrix, intravasation and extravagation of cells in and out of the blood stream, and the growth of secondary tumors in distant organs. The initial event in cancer invasion involves the breaching of the basement membrane, which separates the epithelial compartment from the surrounding collagenous matrix. Cells can leave the primary tumor either individually or collectively [65]. Clinical trials using protease inhibitors failed to completely diminish metastasis and mortality, suggesting that cells can invade through mechanisms other than chemical degradation. In fact, developmental models have shown that cells can breach through a basement membrane using mechanical remodeling of the matrix in salivary glands [11], mouse embryos [38] and *C. elegans* [40].

The process of cancer cell invasion in general has been extensively studied. However, using microscopy techniques to discover what mechanisms cancer cells in a spheroid use to breach the basement membrane and to cross over into the surrounding collagenous matrix, has been limited. This limitation is partly due to the lack of available *in vitro* 3D-tumor models for microscopy techniques. Since 3D imaging is challenging and requires microscopes equipped with long working-distance objectives to image three-dimensional spheroids in collagen gels, as well as live-imaging capabilities for imaging over long periods of time. Additionally, *in vivo* models are challenging for study basement membrane breaching since invasion is rare, unpredictable, and occurs deep

in the body. Moreover, *in vivo* tumor models often lack a continuous basement membrane to use for studying cell-basement membrane dynamics. To overcome these challenges, our laboratory has created a three-dimensional spheroid model enclosed within a basement membrane, which is then embedded in a collagen gel for three-dimensional invasion microscopy studies [41].

Our laboratory has previously shown that single fibroblastic cells can deform collagen matrix by applying traction force to the fibrillar collagen [66]. In spheroid models, it was previously shown that collectively, spheroids can exert force on a three-dimensional polymer network to facilitate tumor invasion [67-69], but these latter findings were not fully investigated mechanistically. What remains to be understood is how human cancer spheroids interact in 3D with the matrix in their immediate surroundings, specifically the basement membrane that separates the cell compartment from the surrounding extracellular matrix (ECM) and then the collagenous ECM matrix.

We have discovered that cells send out long, slender, actin-based protrusions stabilized by tubulin through the basement membrane. These protrusions attach to collagen fibrils using the integrin  $\alpha 2\beta 1$  and mechanically pull and displace the surrounding collagen matrix using myosin II contractility.

## Results

### ***Long cellular protrusions traverse the basement membrane before and during invasion and may apply traction to the surrounding matrix during BM breaching***

We discovered that cells in a spheroid encapsulated by a BM initially send out protrusions starting at approximately 10 hours increasing to 32 hours, accompanied by inward movement of the surrounding collagen gel (Figure 4.1A). These findings suggest that cells may use these long protrusions to provide force to displace collagen during cancer invasion. Moreover, following the red arrow in collagen, we observed that when the protrusions protrude through the basement membrane, the collagen starts to be pulled toward the spheroid. This is shown by the translocation of the two objects marked with red arrowheads in Figure 4.1 in the collagen gel that are being pulled toward the spheroid. Using fluorescence microscopy, we confirm that spheroids with a basement membrane display long cellular protrusions (~30-100  $\mu\text{m}$ ) that penetrate through the basement membrane before cell invasion and extend out into the collagen gel (Figure 4.1B-left panel). During basement membrane breaching by the cancer cells, we find that the long protrusions still exist (Figure 4.1B-middle panels), as well as after the cells have already traversed the basement membrane (Figure 4.1B-right panel). These findings suggested that the protrusions were pulling inward toward the spheroid to facilitate outward cell translocation to breach the basement membrane and permit outward invasion.

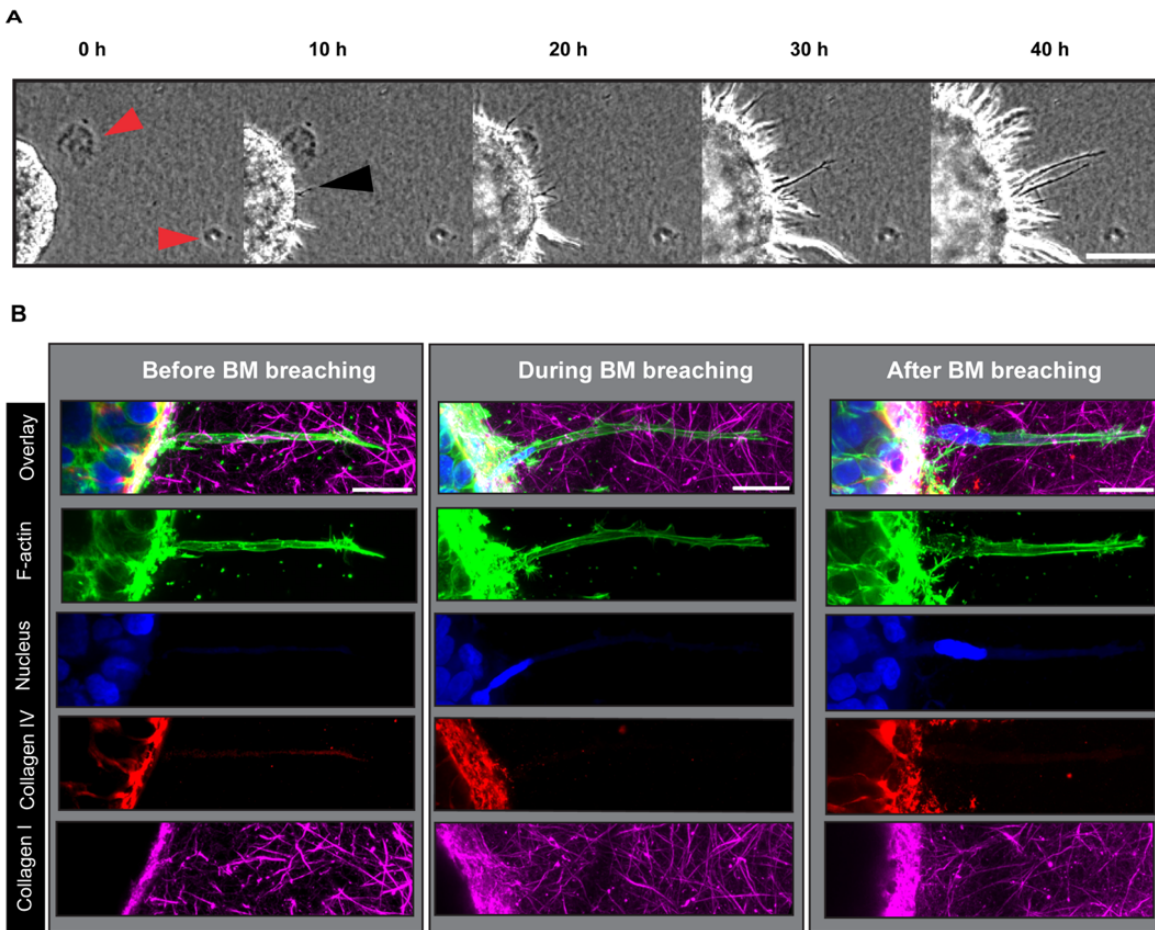


**Figure 4.1. Timelapse live imaging of the spheroid invasion assay with confocal Imaging of long protrusions breaching the basement membrane**

(A) We generated a video montage from timelapse brightfield live imaging of MDA-MB-231BO spheroids. The red arrowheads mark points of reference in the first image that move toward the spheroid as invasion occurs. Additionally, at time 0h there are no protrusions, then at 10 hours there are more protrusions forming with the black arrowhead marking a protrusion of interest that extends through time into the surrounding collagen gel as the collagen is being pulled toward the spheroid. (B) Confocal immunofluorescence microscopy of long protrusions that extend out of the

basement membrane and into collagen gel before, during, and after cell breaching of the basement membrane (note the locations of the blue nuclei). Collagen I accumulates on the outer surface of the spheroid, shown by the increase in signal brightness of pre-labeled collagen I molecule, indicating that the cells may have pulled the matrix toward the base of the spheroid in the presence of protrusions but prior to cellular invasion (left panel). Scale bars: (A), 100  $\mu\text{m}$ ; (B), 20  $\mu\text{m}$ .

***Cells pull on the surrounding collagen matrix through the basement membrane using myosin II***

To quantify the direction and extent of translocation of surrounding collagen matrix, we imaged spheroids surrounded by a basement membrane using brightfield microscopy over 63 hours, taking images every 15 minutes. From the live-imaging timelapse videos, we generated kymographs of regions of interest (Figure 4.2A), which confirmed that the collagen was translocated toward the spheroid over time. In a magnified view of initial times of the kymograph, we observed the protrusions extending into the collagen gel as the collagen was being pulled inward (Figure 4.2A-1). These protrusions became accompanied by cells moving outward, into the collagen gel (Figure 4.2A-2), eventually leading to collective cell migration or streams of cells leaving the expanding spheroid and invading into the collagen gel (Figure 4.2A-3).

To further analyze whether this inward collagen translocation is mechanical, we hypothesized that the cells were pulling on the matrix using myosin II. We treated the cells with a small-molecule inhibitor of myosin II (blebbistatin) and imaged the spheroid for 18 hours. Generating kymographs from the 18-hour timelapse videos (Figure 4.2C-D) demonstrated that when the spheroids were treated with blebbistatin, collagen displacement was significantly decreased compared to control spheroids that were treated with the DMSO vehicle (Figure 4.2C-D). Quantification showed that the cancer cells displace collagen at an average rate of  $\sim 20 \mu\text{m}$  per 18 hours on average, but when treated with the myosin II inhibitor, collagen displacement decreased to an average of only  $\sim 2 \mu\text{m}$  over the 18-hour assay period. Importantly, the cancer cells of blebbistatin-treated spheroids also showed strong inhibition of outward cell migration and invasion

compared to controls (Figure 4.2B). That is, the loss of collagen displacement in blebbistatin-treated spheroids is linked to suppression of cell invasion, supporting our hypothesis that the cancer cells are using myosin II contractility to pull their cell body through the BM and into the collagen matrix during invasion.

To further analyze whether there is actual tension on the collagen mediated by each protrusion that results in collagen displacement over time, we conducted a cell-ablation experiment (Figure 4.3). Using two-photon confocal live-cell imaging microscopy, we ablated single long protrusions that associated with collagen fibrils, and we imaged for 60 seconds from the time of ablation. We then generated a kymograph to measure collagen relaxation through time after severing the protrusion (Figure 4.3C). We found that there were reproducible, rapid collagen gel displacements within 2 seconds after laser ablation consistent with loss of tension being held by the single protrusion (Figure 4.3D). Thus, each protrusion pulls on and displacing the collagen the equivalent of approximately 1  $\mu\text{m}$ . Since multiple individual protrusions are involved in such displacements, these findings support our hypothesis that the protrusions are displacing the collagen toward the spheroid, which would facilitate outward cell invasion.

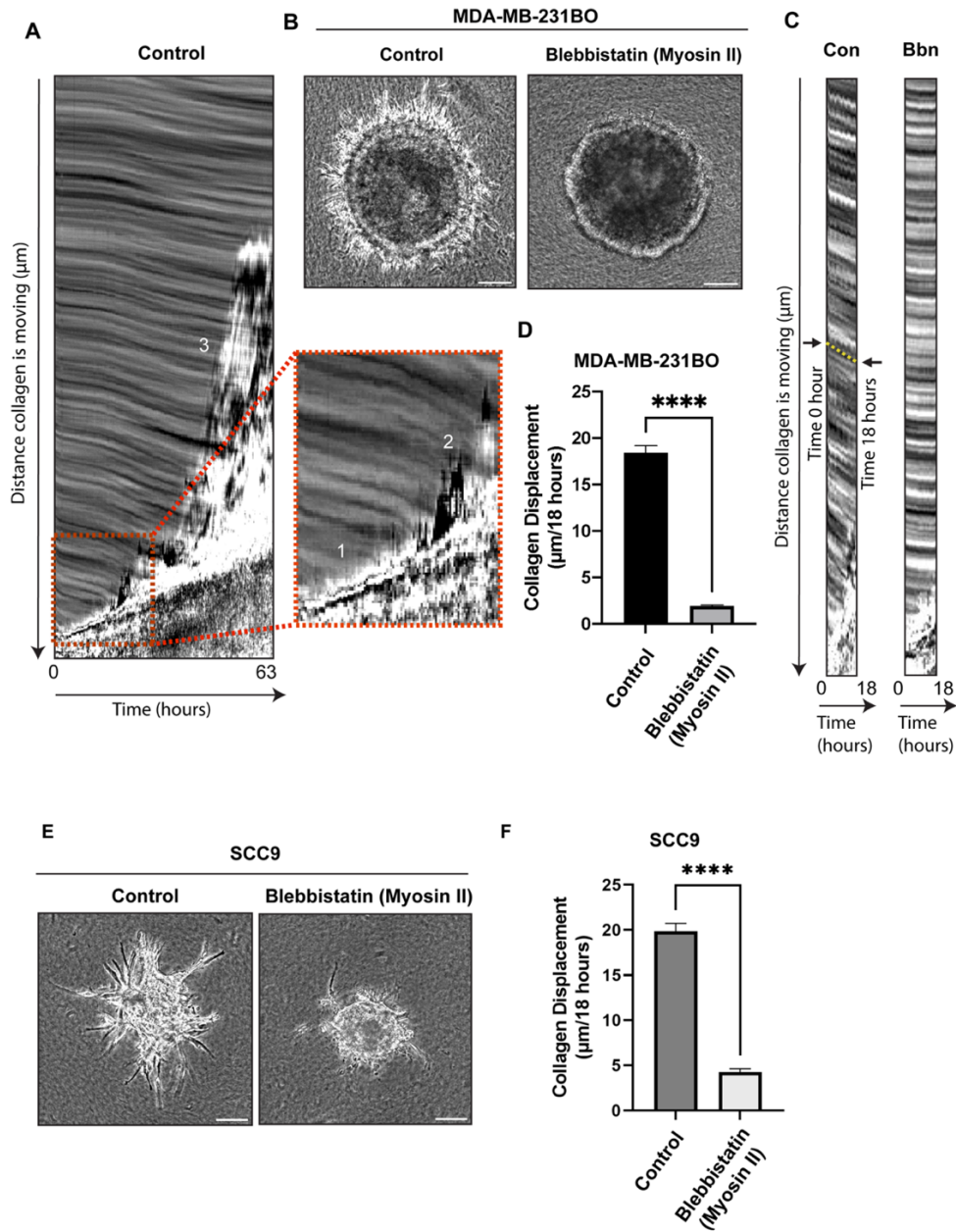


**Figure 4.2. Collagen displacement requires myosin II contractility as does subsequent cell invasion**

(A) Kymograph image of a region of interest of a timelapse video of spheroid cancer cells invading through a basement membrane and into the surrounding collagen gel over 63 hours. The x-axis shows the time in hours and the y axis the distance of

collagen gel displacement in  $\mu\text{m}$ . The magnified image shows protrusions from the spheroid surface that appear to result in collagen moving inward (magnified-region 1), as well as cells invading through the BM zone (magnified-region 2), and then a stream of cells going through the collagen gel (main image-region 3). (B) Spheroids were treated as a control with the DMSO vehicle, which did not affect cancer cell invasion through the BM, or with the myosin II ATPase inhibitor blebbistatin, and were imaged with timelapse phase contrast microscopy over 18 hours. (C) From the timelapse imaging of the control (Con) and blebbistatin (Bbn) groups, we generated kymographs to quantify collagen displacement over time. (D) Collagen displacement was dramatically inhibited by the myosin II inhibitor compared to its control. (E) An oral cancer cell line, SCC9, was used to generate spheroids for comparisons with the MDA-MB-231BO cell line. The SCC9 spheroids were treated with the myosin II inhibitor blebbistatin or control vehicle and were imaged for 36 hours using timelapse live imaging. The SCC9 spheroids were imaged for a longer time period because they invade more slowly through the matrix than the MDA-MB-231 cell line shown in panel B. (F) As previously described, we imaged spheroids over time and prepared a montage from the live timelapse imaging data. We then quantified collagen displacement compared to control. \*\*\*\*  $p < 0.0001$ . Scale bars: (B) and (E), 100  $\mu\text{m}$ .

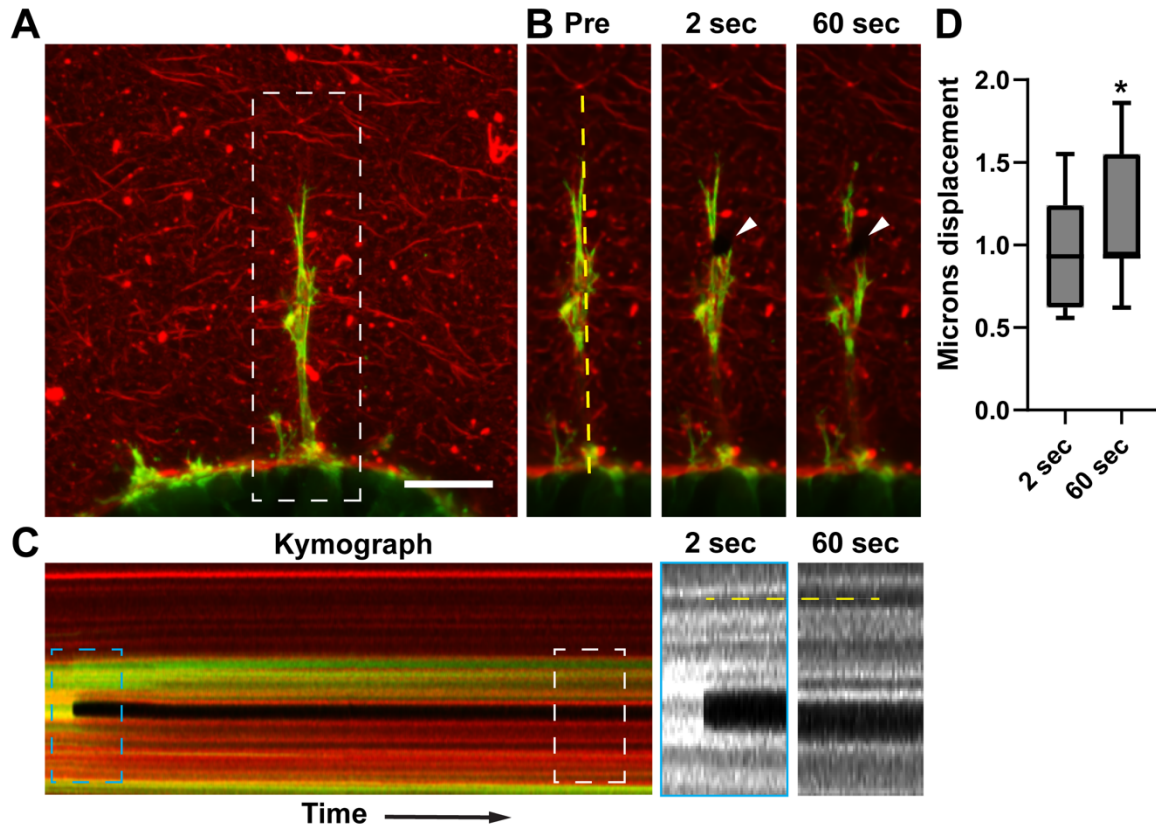


**Figure 4.3. Extending long protrusions generate tension within the collagen microenvironment.**

(A) 8 hours after embedding spheroids in collagen gels, MDA-MB-231BO cells expressing mNeon Green lifeAct (green) form protrusions into the surrounding collagen matrix (red). The image is a maximum intensity projection of 10  $\mu\text{m}$ . Scale bar: 25  $\mu\text{m}$ .

(B) The same cell (white dashed box in panel A) shown only at a single Z plane immediately before (Pre) and at 2 and 60 seconds after a focused 2-photon beam severs the protrusions (arrowheads). Vertical yellow dashed line indicates position of the kymograph shown in panel C. C) Kymograph depicts the time of protrusions severing (black stripe) and the relatively small release of tension within the ECM after protrusions collapse. Cyan and white dashed boxes (magnified on the right) illustrate

the subtle changes 2 and 60 seconds after cell and ECM severing. Vertical dashed yellow line demonstrates a small change at 2 seconds following by continued ECM relaxation over 60 seconds. D) Analysis of protrusions severing at 2 and 60 seconds. N=9, n=48. \*  $P \leq 0.001$ .

***Actin polymerization and tubulin are necessary for long protrusion formation and stabilization of the protrusions for collagen displacement and ultimately cell invasion***

Immunofluorescence staining showed that the long, potentially prehensile protrusions were actin based. To test whether these protrusions are responsible for the pulling force on the collagen matrix, we directly inhibited actin polymerization using two actin inhibitors, latrunculin A and cytochalasin D, which resulted in disappearance of the protrusions dramatic inhibition of collagen displacement (Figure 4.4A). Other actin cytoskeletal inhibitors targeting actin-associated proteins such as CDC42, fascin, Arp2/3, and ROCK (Rho-associated protein kinase), also significantly decreased collagen displacement and invasion compared to controls (Figure 4.4A-B). We then investigated whether these long protrusions are also stabilized by some other cytoskeletal structure. Treatment of spheroids with the tubulin inhibitor nocodazole inhibited the formation of long protrusions, as well as inhibiting collagen displacement (Figure 4.4A-B). In another experiment to test for a role in stabilization of protrusions, we permitted spheroids to form long protrusions and then treated with nocodazole to examine for destabilization. After treatment for one day, the long protrusions started to shorten in a timelapse live imaging experiment (data not shown).

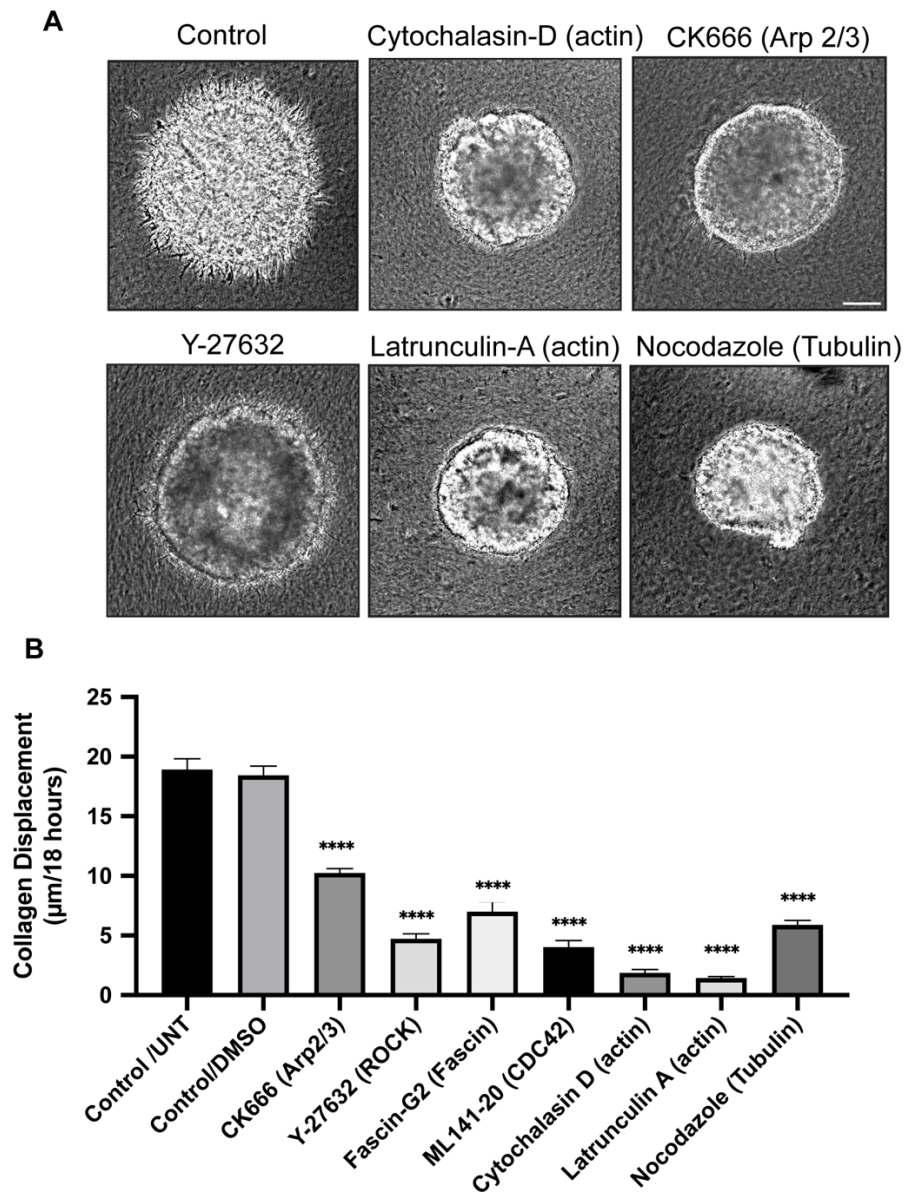


**Figure 4.4. Quantitative comparison of effects of actin polymerization inhibitors on rates of collagen displacement.**

(A) Representative images of spheroids treated with different inhibitors that directly or indirectly affect actin polymerization. The control is DMSO vehicle-treated spheroids. The spheroids were imaged using live-timelapse phase contrast microscopy over 18

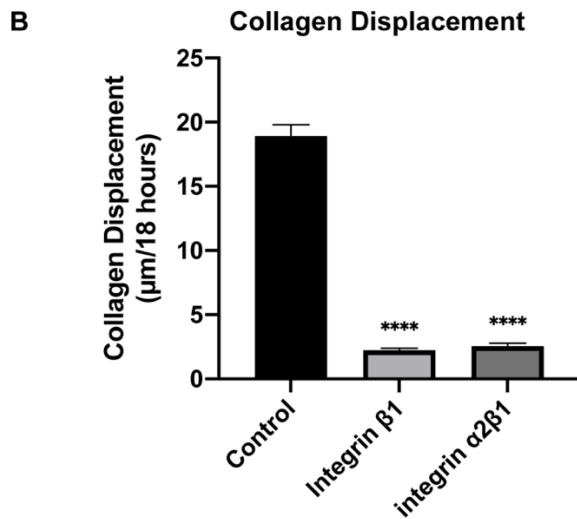
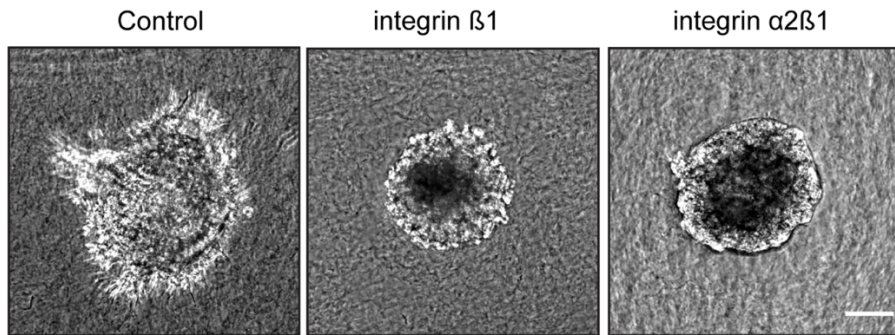
hours. (B) Kymographs were generated from each treatment and control group and the

distance that collagen traveled from time 0 to 18 hours was measured and quantified as collagen displacement. These images and graphs are based on pooled data from at least 3 independent experiments, each including at least 3 spheroids per experiment; similar results were seen in all 3 experiments. Collagen displacement was measured from six computer-selected regions surrounding each individual spheroid. \*\*\*\*  $p < 0.0001$ . Scale bar 100  $\mu\text{m}$ .

***Long protrusions attach to collagen via integrin  $\alpha2\beta1$  to translocate the matrix during spheroid invasion***

To test whether these protrusions attach to collagen in a prehensile-like manner to ultimately translocate the matrix, we tested several different anti-functional integrins for their effect on collagen displacement and cell invasion. We found that the inhibition of an integrin subunit shared broadly with multiple integrin  $\alpha$  subunits, integrin  $\beta1$ , substantially decreased numbers of protrusions, collagen displacement, and cell invasion (Figure 4.5A). Interestingly, inhibition of the collagen-binding integrin  $\alpha2\beta1$  also significantly inhibited protrusion attachment to collagen, thereby impeding collagen displacement and cell invasion. These findings indicate that the cancer cells are attaching to collagen via  $\alpha2\beta1$  to apply pulling forces during invasion.

**A Spheroids after 18 hours of treatment with anti-functional integrin antibodies**

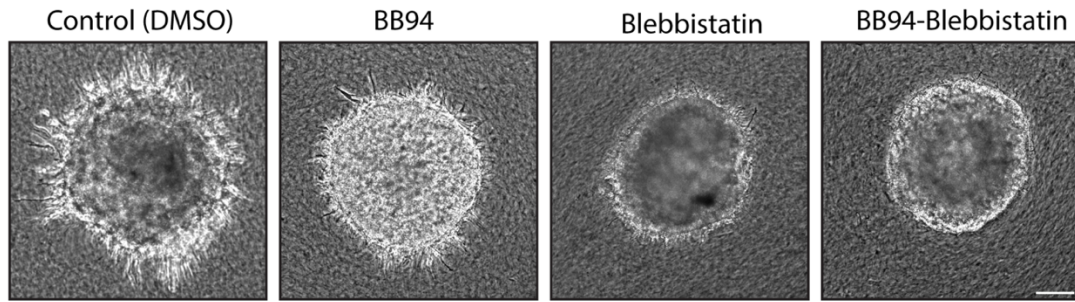
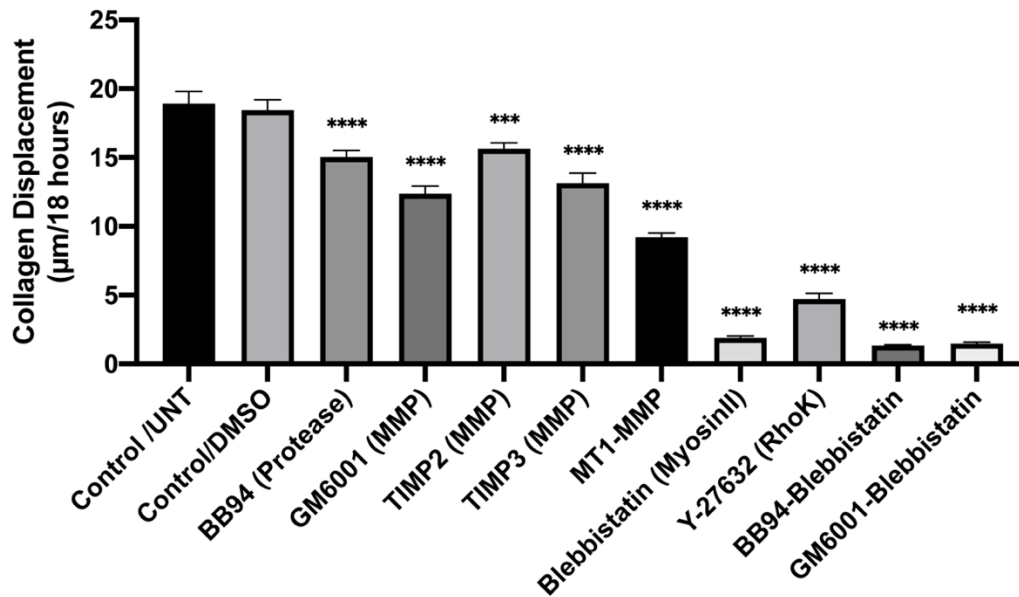


**Figure 4.5. Quantitative demonstration that the protrusions attach to collagen matrix via  $\alpha2\beta1$  integrin.**

Spheroids were treated with anti-functional antibodies to integrins that anchor to collagen and were imaged over 18 hours using phase contrast microscopy. (A) Representative images of inhibition by integrin  $\beta1$  and  $\alpha2\beta1$  anti-functional antibodies of spheroid invasion into collagen gels compared to controls. (B) Using 18-hour timelapse imaging files, we generated kymographs as described for Figure 4.2, measuring the distance that the collagen was translocated from time 0 h to 18 h. \*\*\*\*  $p < 0.0001$ . Scale bar: 100  $\mu\text{m}$ .

### ***The role of proteases in protrusion formation, collagen displacement, and cell invasion***

We had previously established that inhibition of proteases, particularly MMPs, suppressed the formation and enlargement of perforations in the BM, which blocked the translocation of cancer cells through the BM [58]. However, it was not clear whether the long protrusions described here still formed and protruded through small BM holes, and whether they could still displace collagen, because the cells still retained myosin II contractility. In fact, we find persistence of protrusions and a large amount of collagen displacement, but low cell invasion (Figure 4.6A-B). In contrast, as noted previously, cells retain some protrusions but fail to pull on and translocate the collagen matrix, and they cannot translocate their cell bodies to invade into the surrounding collagen (Figure 4.6A-B). Combining inhibition of proteases and myosin II contractility suppresses both collagen displacement and cancer cell invasion into the collagen gel.

**A****B**

**Figure 4.6. The role of proteases in spheroid protrusion formation, collagen displacement, and invasion.**

(A) Representative images of spheroids after 18 hours of treatment with a broad protease inhibitor (BB94), and/or myosin inhibitor (blebbistatin) and their effects on cell invasion. (B) From the timelapse live imaging, we generated kymographs to quantify collagen displacement after treatment with broad-spectrum protease inhibitors, tissue inhibitors of metalloproteinases (TIMPs 2 and 3), contractility inhibitors of myosin II and ROCK, and combinations of BB94 and GM6001 with blebbistatin (B). \*\*\*\*  $p < 0.0001$ ,

\*\*\*  $p < 0.0008$  The images and graph shown here are from pooled data of at least 3 independent experiments with at least 3 spheroids per experiment, all of which showed similar effects. Scale bar: 100  $\mu\text{m}$ .

### ***Characterizations of the long, prehensile-like, contractile protrusions***

The long, thin cellular protrusions from cancer cell spheroids through basement membranes vary in length and diameter, e.g., often 30-100  $\mu\text{m}$  in length and  $\sim 2\text{-}3$   $\mu\text{m}$  in diameter. It should be noted that these protrusions sometimes can have lateral blebs. Using electron microscopy, we observed not only microtubules, but also vesicles of varying sizes, mitochondria, and ER (endoplasmic reticulum) in the long protrusions. With immunofluorescent confocal microscopy we confirmed that mitochondria and ER are present in the long protrusions with no obvious concentration at either end. Microtubules were also observed using electron microscopy as shown previously (Figure 4.7B) and by using immunofluorescence staining (Figure 4.7B). Microtubules were observed along the protrusion, and our inhibition studies suggest that they may act to support those long structures, since microtubule disruption of pre-existing long protrusions results in gradual retraction (data not shown). Our inhibition studies showed that myosin II is important for collagen displacement (Figure 4.1A-B) and we confirm robust immunofluorescence staining for myosin IIA and IIB in the protrusions. In a study using the CRISPR knockout cell pools of Myosin IIA or myosin IIB, we found that both knockout significantly inhibited collagen displacement (data not shown), however, the MDA-MB-231 cell line has significantly more myosin IIA expression [66] (Doyle, 2021, Figure S6B) which could be signify that myosin IIA may play a more vital role in collagen displacement compared to myosin IIB. Interestingly, we could not detect in these protrusions any myosin X (Figure 4.7B), which is a marker for filopodia. As expected, they also immunostain well for integrins including  $\alpha 2$  and  $\beta 1$  (data not shown). Therefore, these long, slender protrusions may not be related to filopodia, consistent

with their content of mitochondria, ER, and vesicles. These long thin cellular extensions instead appear to be a slender arm-like, force-generating extension of the cytoplasm packed with contractile, energy-generating, and supportive elements with abundant cell surface integrins for gripping fibrillar collagen.

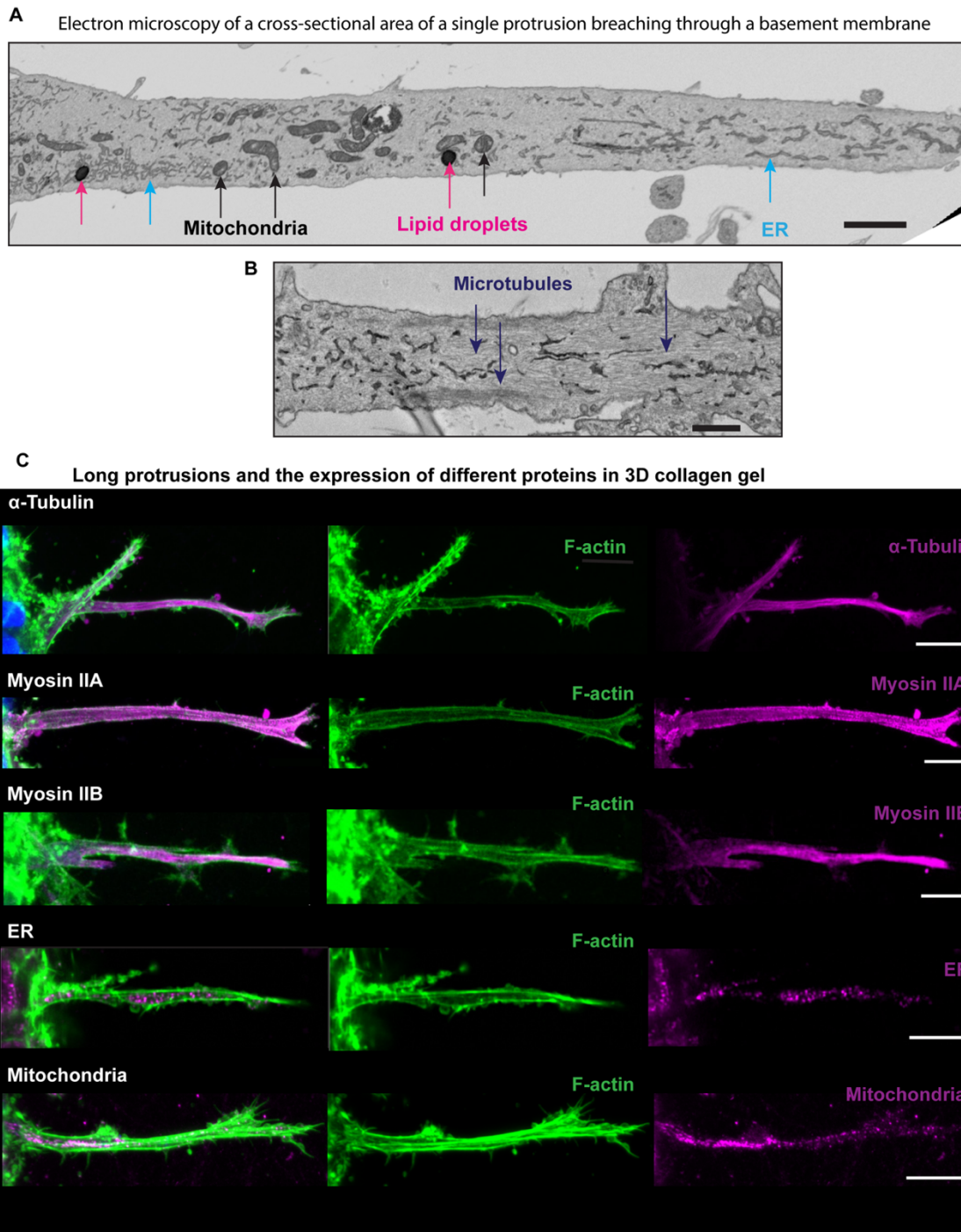


**Figure 4.7. Characterizations of the long protrusions.**

(A) Representative images of the long cellular protrusions in 3D collagen gels (gel not shown for clarity), using electron microscopy showing organelles such as endoplasmic reticulum (ER) and mitochondria (A) and microtubules (B). (C)

Representative images of Immunofluorescence staining of various organelles and cytoskeletal proteins analyzed in the inhibition studies shown previously or observed by electron microscopy imaging (B). Scale bars: (A), 2  $\mu\text{m}$ ; (B), 1  $\mu\text{m}$ ; (C), 10  $\mu\text{m}$ .

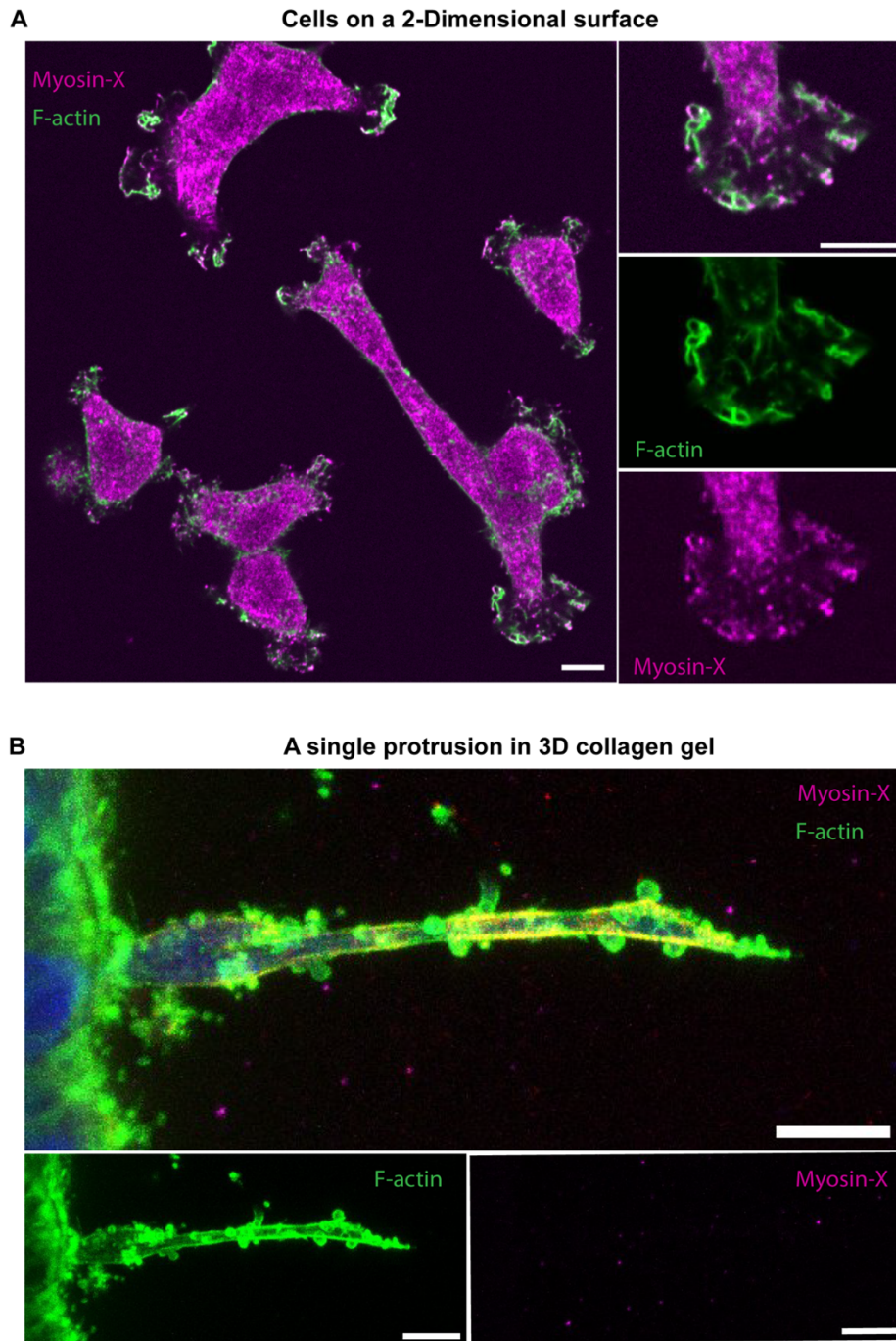


**Figure 4.8. Absence of myosin-X expression in the long thin protrusions.**

(A) Although myosin X can be readily detected in the filopodia of cells on a 2-dimensional surface, (B) it could not be detected in the long invasive protrusions in 3D collagen gels. Scale bar: (A) and (B) 10 $\mu$ m.

## Discussion

In this study, we used our three-dimensional spheroid model with an encapsulating basement membrane that is embedded in collagen gels to observe that cancer cells send out unusually long, slender protrusions through the basement membrane to displace collagen toward the spheroid during invasion. Previous studies using single cells found that cancer cells can exert forces on collagen fibrils to move during cell migration. *In vivo* models of cancer progression have documented the reorganization of collagen fibrils, changing from parallel to perpendicular to the tumor boundary during cancer invasion [9]. This reorganization could suggest that tumor cells are exerting force on the surrounding collagen that result in re-alignment of the fibrils to promote invasion. *In vitro* spheroid models have pointed to this force originating from collective tumor cells [67-69] but little is known about the mechanisms of such invasion.

We report that cells send out long, slender actin-based protrusions through the basement membrane that are stabilized by microtubules. These protrusions attach to the adjacent fibrillar collagen gel via integrin  $\alpha2\beta1$  and displace collagen toward the spheroid using myosin II contractility, and they are finally able to translocate their cell bodies through the basement membrane and invade. In a previous publication, we described how cells perforate and expand holes in the basement membrane during cancer invasion [58]. We propose a model that cells initially poke small holes in the basement membrane using their short actin-based protrusions and proteases. They lengthen their actin-rich protrusions that are stabilized by microtubules to extend through the small perforation in the basement membrane and into the surrounding

collagen gel. Then then attach to the collagen gel via integrin  $\alpha2\beta1$  while they are still within the initial small holes in the basement membrane. They finally pull themselves through the small perforation using myosin II and proteases to translocate their cell bodies through the basement membrane during cancer cell invasion.

## CHAPTER 5:

### Conclusion and Perspective

Understanding the very early events in basement membrane breaching and cell-ECM interactions during cancer invasion is important in discovering solid tumor therapies. Basement membrane breaching is the initial step in solid cancer invasion, leading to cancer cell dissemination, metastasis, and higher mortality rates. Basement membrane breaching was initially thought to only occur by chemical degradation via proteases, such as MMPs. However, many clinical trials using broad and specific protease inhibitors failed to completely suppress metastasis [31, 70], suggesting that cancer cells could invade through other mechanisms. Our laboratory and others have previously shown that cells can cross a basement membrane *in vivo* using mechanical reorganization of the basement membrane [11, 14, 38].

In this dissertation, we sought to understand and decipher the dynamics of cancer cells invading in a collective manner into their collagenous extracellular matrix, traversing through the basement membrane that separates the epithelial from the stromal compartments. While there are stromal cells that have been shown to contribute to matrix remodeling during invasion, such as CAFs and immune cells, the contribution of cancer cells themselves in a collective form (i.e., spheroids or organoids) in basement membrane breaching is not yet clear. This is partly due to the lack of robust three-dimensional cancer invasion models that can be used for microscopy and live imaging. It is difficult to study cell-basement membrane interaction *in vivo* because of the rarity of detecting the time of basement membrane breaching as well as the

limitations for conducting imaging studies because of the limited working distance of microscope objectives. Moreover, most human and mouse tumors, when removed, already lack a continuous basement membrane that can be used to study cell-basement membrane interactions. To overcome these challenges, we created a three-dimensional in vitro model to mimic a simple tumor microenvironment to study the interactions of cancer cells with its immediate surrounding extracellular and basal matrices, while being able to fully image these spheroids over time using confocal microscopy [41].

With our three-dimensional invasion model, we found that cancer spheroids encapsulated in a basement membrane and embedded in collagen gels perforate their basement membrane, and then expand these perforations over time during cancer invasion. When the perforation was smaller than the diameter of a cell,  $\sim 10 \mu\text{m}$ , invasion was minimal. But over time, as the perforations expanded over a size threshold, the cells invaded more effectively into the surrounding collagen gel.

They first use their protrusions and proteases to poke small holes and then to expand these holes. When treated with a variety of protease or actin inhibitors, we found that perforations in the BM were significantly smaller, and invasion was also inhibited compared to controls. In other words, cells that cannot expand their perforations in the BM cannot invade outward. Myosin II contractility also had a significant effect on basement membrane perforation expansion, although this effect was less than proteolysis or actin polymerization. Instead, we found a particularly important role for actin polymerization, which we found to be crucial for cell protrusions to expand BM perforation areas to be able to invade; in comparison, there was a lesser requirement for actomyosin contractility than was previously shown in developmental

models. Therefore, the joint functions of proteolysis and actin polymerization were both important for BM perforation expansion and cancer basement membrane breaching to mediate cancer invasion.

Our timelapse live imaging and confocal imaging of our three-dimensional tumor spheroids revealed that cells generate long, slender protrusions over time that reach through the basement membrane, which is accompanied by an inward movement of matrix during cancer invasion. We imaged these spheroids with a basement membrane that were embedded in collagen gels for over a time span of 18 hours, and then created kymographs with the timelapse videos. Using these kymographs, we were able to quantify how much the collagen gel was moving inward or displacing toward the spheroid over time. We were also able to visualize when this collagen movement is occurring and whether this occurs concurrently with the presence of protrusions reaching through the basement membrane. To understand whether cells pull on the collagen mechanically, we inhibited myosin II, which resulted in a dramatic inhibition of collagen displacement in our MDA-MB-231BO cell line as well as with the oral cancer SCC9 cell line. These findings suggest that the cells are mechanically pulling the matrix toward them during invasion.

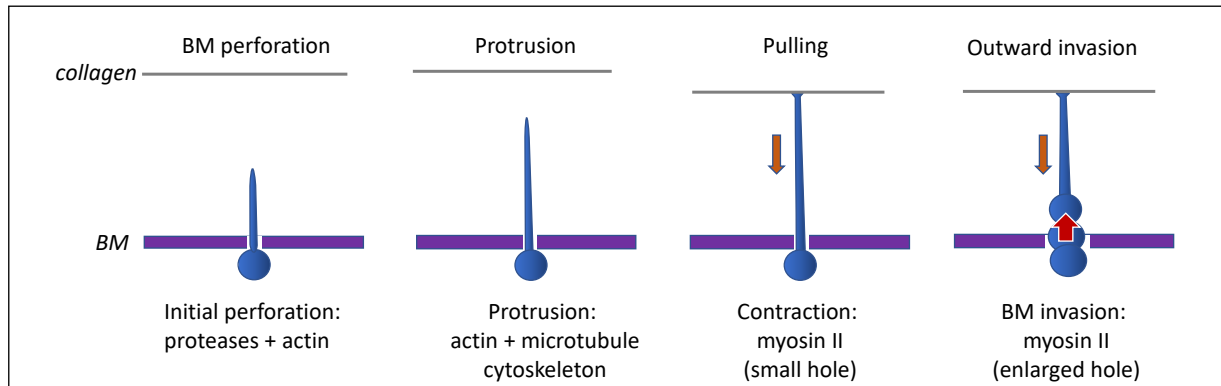
To investigate if these protrusions are pulling on the matrix, we inhibited actin polymerization and observed that there were no apparent long protrusions and concomitantly almost no collagen displacement. We hypothesized that these long structures may be stabilized by microtubules because when we allowed the protrusions to extend through the BM and then added nocodazole, a tubulin inhibitor, we observed through timelapse imaging that these long protrusions shorten over time. To further

investigate whether these protrusions are attaching to the collagen gel as they reach through the basement membrane, we used anti-functional antibodies against different integrins known to be receptors for collagen. We found that when we inhibit integrin  $\alpha 2\beta 1$ , we suppressed the formation of long protrusions. Additionally, collagen displacement and cell invasion are both dramatically inhibited with  $\alpha 2\beta 1$  inhibition. These results indicate that integrin  $\alpha 2\beta 1$  is necessary for protrusion attachment and collagen displacement leading to cancer invasion. Lastly, inhibiting a range of proteases and MMPs affected collagen displacement, but the collagen was still being pulled inward. From our previous publication [58], we infer this is due to the fact that the perforations are smaller than the diameter of a nucleus (the largest part of a cell), so while the cell cannot fully transmigrate through the basement membrane, it can still extend a protrusion outward because of actin polymerization and tubulin, and thus pull the matrix inward by myosin II contractility.

There are still several questions that need to be addressed in the future: Which non-muscle myosin II isoform is actually driving collagen displacement? Is myosin IIA or IIB more important in collagen displacement and pulling? Are mitochondria and ER necessary for the invasive function of these protrusions? Does the thickness of the protrusion indicate more pulling force on the collagen gel? In addition to conducting experiments to address these questions, we also hope to perform single-cell sequencing to examine for differences in gene expression between cells that are pulling and the cells that trail behind. Perhaps there is something unique about these leader cells during invasion. In our experience, the isolation of cells with long protrusions from the 3D gels would be technically difficult, but these findings would be valuable,

nevertheless. A suggestion could be for pathologists to search carefully for thin but long protrusions near *in situ* tumors, since we observed in our MDA-MB-231, SCC9, and 4T1 cells that they send out long protrusions to displace the collagen through the BM.

Nevertheless, our studies have successfully established the concept that cancer spheroids encapsulated in a basement membrane and embedded in collagen gels penetrate through the basement membrane using proteases and by sending out long actin-based protrusions into the surrounding matrix. They lengthen these protrusions that are stabilized by microtubules and attach to the collagen using integrin  $\alpha 2\beta 1$ . These protrusions can then pull the matrix inward using myosin II contractility and can concomitantly ultimately pull themselves through the BM hole using actin polymerization and myosin II to translocate their nucleus and the remainder of their cell bodies during invasion.



**Scheme 5.1. A model of basement membrane invasion.** The cancer cell within a spheroid, depicted as a single cell in blue for simplicity, perforated the basement membrane (purple) via its actin-based protrusion and proteolysis. The cell then extends this actin-based protrusion that is supported by tubulin and reaches into the collagen gel and attaches to the collagen fibrils via integrin  $\alpha 2\beta 1$ , while still in a small hole (smaller than a diameter of a cell). The protrusion then pulls the collagen gel fibrils toward itself via myosin II contractility. Finally, the cell can expand the basement hole to translocate its nucleus and cell body to invade via further proteolysis and myosin II contractility and perhaps allow for additional cells to trail behind during collective cancer cell invasion.

## MATERIALS AND METHODS

### *Cell Culture and Media*

We used MDA-MB-231 Bone (MDA-MB-231BO) cells originally described in [49] and obtained from Dr. Kandice Tanner, National Cancer Institute. The culture medium used was Dulbecco's MEM (DMEM; Gibco) with 10% FBS (Life Technologies), 1% penicillin/streptomycin (Life Technologies), and 1% L-glutamine (Life Technologies). Media were sterile filtered through 0.45  $\mu\text{m}$  nitrocellulose filters. Cells and spheroids were maintained in a humidified 10% CO<sub>2</sub> incubator at 37 °C.

### *3-Dimensional Spheroid Cell Culture*

Detailed protocols for this method were published previously [41] and are illustrated in Scheme 1. Briefly, MDA-MB-231 BO cells were seeded at a 500 cells-per-well density in ultra-low attachment V-bottom (or U-bottom) 96 well plates (PrimeSurface from s-Bio). After 8 h at 37 °C, the plate was centrifuged for 5 min at 300 RPM and placed back into the tissue culture incubator for 48 h to permit the cells in the spheroid to form a compact spheroid via cell–cell adhesion. We then added a final concentration of Matrigel diluted to 5% in medium per well and centrifuged for 5 min at 300 RPM. The plate was then incubated for at least 48 h further to induce basement membrane assembly around the spheroid. The spheroids were then washed in cold HBSS (Hanks balanced salt solution, Life Technologies) at least 3 times and embedded in 4.0 mg/mL rat-tail collagen I gels. The gels were polymerized at 37 °C for 1 h, and serum-containing cell media or imaging media was added to the dish after the incubation period. We had also tested 2 mg/mL collagen gels (Figure 3.7B), but we ultimately chose to use 4 mg/mL gels because they

proved less likely to tear or detach from our MatTek culture dishes during the rigorous washing of our immunostaining protocol.

### *Inhibitors*

For experiments in which spheroids were treated with inhibitors, the spheroids were embedded in neutralized collagen gels and, after polymerization, media were added containing the following treatments: BB94 (5  $\mu$ M), GM6001 (20  $\mu$ M), TIMP2 (4  $\mu$ g/mL), TIMP3 (4  $\mu$ g/mL), Y-27632 (20  $\mu$ M), blebbistatin (20  $\mu$ M), ML141 (20  $\mu$ M), cytochalasin D (2  $\mu$ M), or latrunculin A (200 nM). DMSO was used as the vehicle control for the inhibitors that were dissolved in DMSO.

### *Immunostaining*

Spheroids embedded in collagen gels were fixed using 4% paraformaldehyde in PBS for at least 1 h, then washed with PBS and blocked with 10% donkey serum for at least 1 h. Primary antibody against collagen IV antibody (Millipore), goat host, was added to the dish and incubated at 4 °C overnight. After washing the 3D assay with PBS, embedded spheroids were incubated with secondary antibodies (Jackson ImmunoResearch) IgG Fab donkey Cy5 labeled anti-goat for at least 4 h at room temperature before imaging.

### *Confocal Imaging*

Confocal imaging was performed on a Nikon A1R MP + HD confocal system (Nikon Instruments, Melville, NY, USA) using a 40 $\times$  Apo long working distance (LWD) water

immersion objective (N.A. 1.15). Laser lines of 405 nm, 488 nm, 561 nm, and 640 nm provided illumination for Hoechst, AF 488, Rhodamine Red X, and AF647 fluorophores, respectively. Data were acquired using Galvano mode at 1024 × 1024 with no line averaging. A Z-piezo stage (Physik Instrumente USA, Auburn, MA, USA) allowed for rapid imaging in Z every 0.5 μm over a 200 μm Z distance. NIS-Elements (Nikon, Melville, NY, USA) controlled all equipment. All images shown are maximum intensity projections and were processed using ImageJ/FIJI.

### *Live Cell Imaging*

The brightfield live-cell images were obtained using a Nikon Ti-E inverted microscope (Melville, NY, USA) with motorized stage (Prior) using 10× (N.A. 0.3) and 20× (N.A. 0.75) air objectives. Images were acquired with a Hamamatsu Orca Flash 4.0 CMOS camera. NIS-Elements (Nikon, Melville, NY, USA) controlled all equipment. An environmental chamber (Precision Plastics, Beltsville, MD, USA) kept cells at a constant 37 °C, 50% humidity and 10% CO<sub>2</sub>.

### *Perforation Area Analysis*

To semi-automatically quantify the basement membrane hole number and area, a Fiji (ImageJ) macro was created by ADD and can be found at [https://github.com/addoyle1D/BM\\_Holes](https://github.com/addoyle1D/BM_Holes) (accessed on August 9, 2022). Briefly, a maximum intensity projection (MIP) was defined and created to which an unsharped mask (radius = 15 mask = 0.6) and a Li threshold were applied. A hand-drawn region of interest

(ROI) was created over the filtered MIP to include only holes within the center-bottom region of the spheroid, and holes overlapping the edge of the ROI were excluded (see Scheme 1 for an example ROI). The function, “Analyze Particles” was then used to calculate the hole areas and number, excluding any hole that touched the ROI edge or was less than 1.5 microns. All images were then automatically saved as tiff and csv files.

### *Collagen displacement analysis*

To semi-automatically quantify collagen displacement, a Fiji (ImageJ) macro was created by ADD. In brief, 6 regions of interest were selected automatically by drawing two lines from each corner to corner of the timelapse file and one line in horizontal across the spheroid. The kymograph-maker plugin was then used to create a kymograph of the region over time. This gave us 6 regions in a single spheroid completely picked in a similar manner in each file, for every treatment and control group. These kymographs were then opened in a separate macro where we measured the height of change in collagen from time 0 to 18 hours, similar to Figure 4.2C. We drew 4 lines from time zero to 18 hours on the kymograph and measured the height of change. The lines were drawn from both sides of the spheroid and were picked at a similar region each time, close to the spheroid but not touching the spheroid. This process was semi-automated using a macro written by ADD.

### *Statistics*

We repeated each experiment at least 3 times and each experiment contained at least 3 spheroids. For the perforation area statistical analyses, we used One-way ANOVA with Dunnett's test.

### *Two-photon cell severing*

For two-photon cell severing experiments, a Nikon A1R HD MP system was used (Nikon Instruments). Imaging used a 40X (1.15 N.A.) water immersion objective and 488 nm (0.5-1.5%) and 561 nm (1-2%) laser lines to illuminate TAGGFP2-LifeAct and Atto565-labeled collagen, respectively, using resonant mode and bidirectional scanning at 512X512. NIS-Elements (Nikon) controlled all equipment. Prior to imaging, a line spot was created approximately 10-15 microns behind the protrusions edge. Using ND acquisition functions, three sequences were configured: 1) a pre-severing 3D single timepoint (0.5 micron Z spacing over 40 microns), 2) a single plane cell severing sequence imaged at 7.5 frames/sec for two minutes (a 10 second delay prior to severing), and 3) a post-severing 3D single timepoint (same as the 1<sup>st</sup>). A Coherent Chameleon Vision II two-photon laser was set to 800 nm and 80% power and a single point was chosen and ablated for 2 seconds. Kymographs were created and distances were measured at 2 and 60 seconds after the 2-second ablation.

## REFERENCES

1. Doyle, A.D., S.S. Nazari, and K.M. Yamada, *Cell-extracellular matrix dynamics*. Phys Biol, 2022. **19**(2).
2. Lambert, A.W., D.R. Pattabiraman, and R.A. Weinberg, *Emerging Biological Principles of Metastasis*. Cell, 2017. **168**(4): p. 670-691.
3. Wolf, K., et al., *Multi-step pericellular proteolysis controls the transition from individual to collective cancer cell invasion*. Nat Cell Biol, 2007. **9**(8): p. 893-904.
4. Deakin, N.O. and C.E. Turner, *Distinct roles for paxillin and Hic-5 in regulating breast cancer cell morphology, invasion, and metastasis*. Mol Biol Cell, 2011. **22**(3): p. 327-41.
5. Friedl, P., et al., *Migration of Coordinated Cell Clusters in Mesenchymal and Epithelial Cancer Explants in-Vitro*. Cancer Research, 1995. **55**(20): p. 4557-4560.
6. Schwager, S.C., P.V. Taufalele, and C.A. Reinhart-King, *Cell-Cell Mechanical Communication in Cancer*. Cell Mol Bioeng, 2019. **12**(1): p. 1-14.

7. Lo, C.M., et al., *Cell movement is guided by the rigidity of the substrate*. Biophys J, 2000. **79**(1): p. 144-52.
8. DuChez, B.J., et al., *Durotaxis by Human Cancer Cells*. Biophys J, 2019. **116**(4): p. 670-683.
9. Provenzano, P.P., et al., *Collagen reorganization at the tumor-stromal interface facilitates local invasion*. BMC Med, 2006. **4**(1): p. 38.
10. Carey, S.P., K.E. Martin, and C.A. Reinhart-King, *Three-dimensional collagen matrix induces a mechanosensitive invasive epithelial phenotype*. Sci Rep, 2017. **7**: p. 42088.
11. Harunaga, J.S., A.D. Doyle, and K.M. Yamada, *Local and global dynamics of the basement membrane during branching morphogenesis require protease activity and actomyosin contractility*. Dev Biol, 2014. **394**(2): p. 197-205.
12. Chang, J. and O. Chaudhuri, *Beyond proteases: Basement membrane mechanics and cancer invasion*. J Cell Biol, 2019. **218**(8): p. 2456-2469.
13. Sekiguchi, R. and K.M. Yamada, *Basement Membranes in Development and Disease*. Curr Top Dev Biol, 2018. **130**: p. 143-191.
14. Kelley, L.C., et al., *Adaptive F-Actin Polymerization and Localized ATP Production Drive Basement Membrane Invasion in the Absence of MMPs*. Dev Cell, 2019. **48**(3): p. 313-328 e8.
15. Gaiko-Shcherbak, A., et al., *The Acinar Cage: Basement Membranes Determine Molecule Exchange and Mechanical Stability of Human Breast Cell Acini*. PLoS One, 2015. **10**(12): p. e0145174.

16. Eddy, R.J., et al., *Tumor Cell Invadopodia: Invasive Protrusions that Orchestrate Metastasis*. Trends Cell Biol, 2017. **27**(8): p. 595-607.
17. Ferrari, R., et al., *MT1-MMP directs force-producing proteolytic contacts that drive tumor cell invasion*. Nat Commun, 2019. **10**(1): p. 4886.
18. Murphy, D.A. and S.A. Courtneidge, *The 'ins' and 'outs' of podosomes and invadopodia: characteristics, formation and function*. Nat Rev Mol Cell Biol, 2011. **12**(7): p. 413-26.
19. Linder, S., C. Wiesner, and M. Himmel, *Degrading devices: invadosomes in proteolytic cell invasion*. Annu Rev Cell Dev Biol, 2011. **27**: p. 185-211.
20. Friedl, P. and K. Wolf, *Plasticity of cell migration: a multiscale tuning model*. J Cell Biol, 2010. **188**(1): p. 11-9.
21. Caswell, P.T. and T. Zech, *Actin-Based Cell Protrusion in a 3D Matrix*. Trends Cell Biol, 2018. **28**(10): p. 823-834.
22. Friedl, P. and S. Alexander, *Cancer invasion and the microenvironment: plasticity and reciprocity*. Cell, 2011. **147**(5): p. 992-1009.
23. Yamada, K.M. and M. Sixt, *Mechanisms of 3D cell migration*. Nat Rev Mol Cell Biol, 2019.
24. Lomakina, M.E., et al., *Arpin downregulation in breast cancer is associated with poor prognosis*. Br J Cancer, 2016. **114**(5): p. 545-53.
25. Arjonen, A., et al., *Mutant p53-associated myosin-X upregulation promotes breast cancer invasion and metastasis*. J Clin Invest, 2014. **124**(3): p. 1069-82.
26. Shibue, T., et al., *The outgrowth of micrometastases is enabled by the formation of filopodium-like protrusions*. Cancer Discov, 2012. **2**(8): p. 706-21.

27. Jacob, A. and R. Prekeris, *The regulation of MMP targeting to invadopodia during cancer metastasis*. *Front Cell Dev Biol*, 2015. **3**: p. 4.
28. Artym, V.V., et al., *Dense fibrillar collagen is a potent inducer of invadopodia via a specific signaling network*. *J Cell Biol*, 2015. **208**(3): p. 331-50.
29. Polette, M., et al., *Tumour invasion and matrix metalloproteinases*. *Crit Rev Oncol Hematol*, 2004. **49**(3): p. 179-86.
30. Hotary, K., et al., *A cancer cell metalloprotease triad regulates the basement membrane transmigration program*. *Genes Dev*, 2006. **20**(19): p. 2673-86.
31. Coussens, L.M., B. Fingleton, and L.M. Matrisian, *Matrix metalloproteinase inhibitors and cancer: trials and tribulations*. *Science*, 2002. **295**(5564): p. 2387-92.
32. Pozzi, A., P.D. Yurchenco, and R.V. Iozzo, *The nature and biology of basement membranes*. *Matrix Biol*, 2017. **57-58**: p. 1-11.
33. Wisdom, K.M., et al., *Covalent cross-linking of basement membrane-like matrices physically restricts invasive protrusions in breast cancer cells*. *Matrix Biol*, 2020. **85-86**: p. 94-111.
34. Pandya, P., J.L. Orgaz, and V. Sanz-Moreno, *Modes of invasion during tumour dissemination*. *Mol Oncol*, 2017. **11**(1): p. 5-27.
35. Gaggioli, C., et al., *Fibroblast-led collective invasion of carcinoma cells with differing roles for RhoGTPases in leading and following cells*. *Nature Cell Biology*, 2007. **9**(12): p. 1392-1400.
36. Glentis, A., et al., *Cancer-associated fibroblasts induce metalloprotease-independent cancer cell invasion of the basement membrane*. *Nat Commun*, 2017. **8**(1): p. 924.

37. Bahr, J.C. and S.J. Weiss, *Macrophage-Dependent Trafficking and Remodeling of the Basement Membrane-Interstitial Matrix Interface*. bioRxiv, 2018: p. 364422.
38. Kyprianou, C., et al., *Basement membrane remodelling regulates mouse embryogenesis*. Nature, 2020. **582**(7811): p. 253-258.
39. Ouderkirk, J.L. and M. Krendel, *Non-muscle myosins in tumor progression, cancer cell invasion, and metastasis*. Cytoskeleton (Hoboken), 2014. **71**(8): p. 447-63.
40. Hagedorn, E.J. and D.R. Sherwood, *Cell invasion through basement membrane: the anchor cell breaches the barrier*. Curr Opin Cell Biol, 2011. **23**(5): p. 589-96.
41. Nazari, S.S., *Generation of 3D Tumor Spheroids with Encapsulating Basement Membranes for Invasion Studies*. Curr Protoc Cell Biol, 2020. **87**(1): p. e105.
42. Kaushik, S., M.W. Pickup, and V.M. Weaver, *From transformation to metastasis: deconstructing the extracellular matrix in breast cancer*. Cancer Metastasis Rev, 2016. **35**(4): p. 655-667.
43. Lee, J.Y., et al., *YAP-independent mechanotransduction drives breast cancer progression*. Nat Commun, 2019. **10**(1): p. 1848.
44. Tevis, K.M., Y.L. Colson, and M.W. Grinstaff, *Embedded Spheroids as Models of the Cancer Microenvironment*. Advanced Biosystems, 2017. **1**(10).
45. Ridley, A.J., et al., *Cell migration: integrating signals from front to back*. Science, 2003. **302**(5651): p. 1704-9.
46. Cukierman, E., et al., *Taking cell-matrix adhesions to the third dimension*. Science, 2001. **294**(5547): p. 1708-12.

47. DeFilippis, R.A., et al., *CD36 repression activates a multicellular stromal program shared by high mammographic density and tumor tissues*. *Cancer Discov*, 2012. **2**(9): p. 826-39.
48. Ursin, G., et al., *Greatly increased occurrence of breast cancers in areas of mammographically dense tissue*. *Breast Cancer Res*, 2005. **7**(5): p. R605-8.
49. Yoneda, T., et al., *A bone-seeking clone exhibits different biological properties from the MDA-MB-231 parental human breast cancer cells and a brain-seeking clone in vivo and in vitro*. *J Bone Miner Res*, 2001. **16**(8): p. 1486-95.
50. Provenzano, P.P., et al., *Collagen density promotes mammary tumor initiation and progression*. *BMC Med*, 2008. **6**: p. 11.
51. Fang, M., et al., *Collagen as a double-edged sword in tumor progression*. *Tumour Biol*, 2014. **35**(4): p. 2871-82.
52. Doyle, A.D., *Generation of 3D Collagen Gels with Controlled Diverse Architectures*. *Curr Protoc Cell Biol*, 2016. **72**: p. 10.20.1-10.20.16.
53. Doyle, A.D., *Fluorescent Labeling of Rat-tail Collagen for 3D Fluorescence Imaging*. *Bio Protoc*, 2018. **8**(13).
54. Doyle, A.D., *Generation of micropatterned substrates using micro photopatterning*. *Curr Protoc Cell Biol*, 2009. **Chapter 10**: p. Unit 10.15.
55. Berens, E.B., et al., *A Cancer Cell Spheroid Assay to Assess Invasion in a 3D Setting*. *J Vis Exp*, 2015(105).
56. Li, Q., et al., *3D models of epithelial-mesenchymal transition in breast cancer metastasis: high-throughput screening assay development, validation, and pilot screen*. *J Biomol Screen*, 2011. **16**(2): p. 141-54.

57. Guzman, A., et al., *A novel 3D in vitro metastasis model elucidates differential invasive strategies during and after breaching basement membrane*. *Biomaterials*, 2017. **115**: p. 19-29.
58. Nazari, S.S., A.D. Doyle, and K.M. Yamada, *Mechanisms of Basement Membrane Micro-Perforation during Cancer Cell Invasion into a 3D Collagen Gel*. *Gels*, 2022. **8**(9).
59. Jayadev, R. and D.R. Sherwood, *Basement membranes*. *Curr Biol*, 2017. **27**(6): p. R207-R211.
60. Bosman, F.T., M. Havenith, and J.P. Cleutjens, *Basement membranes in cancer*. *Ultrastruct Pathol*, 1985. **8**(4): p. 291-304.
61. Sirka, O.K., E.R. Shamir, and A.J. Ewald, *Myoepithelial cells are a dynamic barrier to epithelial dissemination*. *J Cell Biol*, 2018. **217**(10): p. 3368-3381.
62. Condeelis, J. and J.W. Pollard, *Macrophages: obligate partners for tumor cell migration, invasion, and metastasis*. *Cell*, 2006. **124**(2): p. 263-6.
63. Tian, B. and P.L. Kaufman, *Comparisons of actin filament disruptors and Rho kinase inhibitors as potential antiglaucoma medications*. *Expert Rev Ophthalmol*, 2012. **7**(2): p. 177-187.
64. Ridley, A.J., *Rho GTPases and actin dynamics in membrane protrusions and vesicle trafficking*. *Trends Cell Biol*, 2006. **16**(10): p. 522-9.
65. Friedl, P. and K. Wolf, *Tumour-cell invasion and migration: diversity and escape mechanisms*. *Nat Rev Cancer*, 2003. **3**(5): p. 362-74.

66. Doyle, A.D., et al., *3D mesenchymal cell migration is driven by anterior cellular contraction that generates an extracellular matrix prestrain*. *Dev Cell*, 2021. **56**(6): p. 826-841 e4.
67. Kopanska, K.S., et al., *Tensile Forces Originating from Cancer Spheroids Facilitate Tumor Invasion*. *PLoS One*, 2016. **11**(6): p. e0156442.
68. Chen, Y.Q., et al., *Early stage mechanical remodeling of collagen surrounding head and neck squamous cell carcinoma spheroids correlates strongly with their invasion capability*. *Acta Biomater*, 2019. **84**: p. 280-292.
69. Mark, C., et al., *Collective forces of tumor spheroids in three-dimensional biopolymer networks*. *Elife*, 2020. **9**.
70. Fingleton, B., *MMPs as therapeutic targets--still a viable option?* *Semin Cell Dev Biol*, 2008. **19**(1): p. 61-8.